Annu. Rev. Nucl. Part. Sci. 2003. 53:301–51
doi: 10.1146/annurev.nucl.53.041002.110601

TOP-QUARK PHYSICS

Dhiman Chakraborty,[1] Jacobo Konigsberg,[2] and David Rainwater[3]

[1]Department of Physics, Faraday Hall West 202, Northern Illinois University, DeKalb, Illinois 60115; [2]Department of Physics, University of Florida, Gainesville, Florida 32611; [3]DESY Theory Group, Laboratory 2a, Notkestrasse 85, D-22603, Hamburg, Germany; email: dhiman@fnal.gov; konigsberg@phys.ufl.edu; rain@mail.desy.de

Key Words heavy fermion, standard model, Tevatron, LHC, top properties

PACS Codes 14.65.HA, 10, 12.60.-I

■ **Abstract** We survey top-quark physics from what has been learned so far at the Tevatron to the searches planned at present and future colliders. We summarize the richness of the measurements and discuss their possible impact on our understanding of the standard model by pointing out their key elements and limitations. We discuss how the top quark may provide a connection to new or unexpected physics. The literature on many of the topics we address is sizeable. We attempt to consolidate the most salient points into a complete, coherent overview.

CONTENTS

1. OVERVIEW

The discovery of the top quark at Fermilab's $p\bar{p}$ collider Tevatron in 1995 by the CDF and DØ collaborations (1) gave direct support to the three-generation structure of the standard model and opened up the new field of top-quark physics. Several properties of the top quark were studied at the Tevatron during its first run. Studies included measurement of $t\bar{t}$ pair-production cross section (2) and kinematical distributions (3–6), measurement of top-quark mass (4–8), tests of the standard model via studies of W helicity in top decays (9) and spin correlations in $t\bar{t}$ production (10), searches for electroweak production of single top quarks (11, 12) and for exotic decays of top such as charged Higgs bosons (13, 14), and searches for flavor-changing neutral currents (15). The precision of most of these measurements is limited by statistical uncertainties because of the small size of the data samples collected so far at the Tevatron (Run 1). Run 2, currently under way, will increase the statistics by approximately two orders of magnitude, while the Large Hadron Collider (LHC) at CERN will be a true top factory, producing tens of millions of top quarks every year (see Table 1). A TeV-scale e^+e^- linear collider would also have sufficient energy to produce top quarks and would be ideal for precision studies of many top-quark properties.

The most striking observed feature that sets the top quark apart from the other quarks is its very large mass. Weighing in at 174.3 ± 5.1 GeV (7), top is about 35 times heavier than the next heaviest quark, bottom (b), and is the heaviest

TABLE 1 Operation parameters of present and future colliders, and cross sections for some important processes

Collider	**Tevatron Run 1**	**Tevatron Run 2**	**LHC**	**LC**
Type	$\boldsymbol{p\bar{p}}$	$\boldsymbol{p\bar{p}}$ 2009	$\boldsymbol{pp}$	$\boldsymbol{e^+e^-}$
Run period	**1992–1996**	**2001–~~2008~~(?)**	**2007–?**	**2015(?)–?**
$E_{\rm cm}$ (TeV)	1.80	1.96	14.0	$<2m_t-\sim1.0$
$\langle\mathcal{L}\rangle$ (cm^{-2}s^{-1})	1×10^{31}	1×10^{32}	10^{33}–10^{34}	2×10^{34}
$\int \mathcal{L}dt$ (fb^{-1})	0.125	~~6.5–11~~ 4.4-8.6	$\sim$300	$\sim$1000
$\sigma_{\rm total}$ (pb)	$\sim 10^{11}$	$\sim 10^{11}$	$\sim 10^{11}$	$O(10)$
$\sigma(b\bar{b})$ (pb)	$\sim 2 \cdot 10^7$	$\sim 3 \cdot 10^7$	$\sim 3 \cdot 10^8$	$O(1)$
$\sigma(WX)$ (pb)	$\sim 3 \cdot 10^4$	$\sim 4 \cdot 10^4$	$\sim 2 \cdot 10^5$	$O(1)$
$\sigma(t\bar{t})$[a] (pb)	$5.19^{+0.52}_{-0.68}$	$6.70^{+0.71}_{-0.88}$	825^{+58}_{-43}	$\sim$0.8
$\sigma(t\bar{t})$[b] (pb)	5.8 ± 0.4	8.0 ± 0.6	—	—
σ(single t) (pb)	1.08 ± 0.01	1.50 ± 0.02	315^{+8}_{-2}	$\sim$0

[a]Complete NLO + NLL calculation.

[b]Partial NNLO + NNLL calculation discussed in Section 2.1.1.

elementary particle known. The top quark, W, and Higgs boson all contribute to radiative terms in theoretical calculations of many observables that have been measured with good precision by the Large Electron-Positron Collider (LEP), the Stanford Linear Collider (SLC), and low-energy neutrino-scattering experiments. Hence, precision measurements of the top-quark mass (m_t) and W mass (M_W) constrain the mass of the standard-model Higgs boson, as shown in Figure 1.

The vast swath of phase space available to the decay of such a heavy quark gives it an extremely short lifetime, about 4×10^{-25} s in the standard model, an order of magnitude shorter than the characteristic hadronization time of QCD, $\tau_{\text{had}} \approx 28 \times 10^{-25}$ s. As a result, the decay of top quarks offers a unique window on the properties of a bare quark free from the long-range effects of QCD, such as confinement.

The large mass of the top quark takes on even greater significance in various extensions of the standard model as particle spectra and flavor- or mass-dependent couplings beyond the standard model are contemplated. Most such particles are

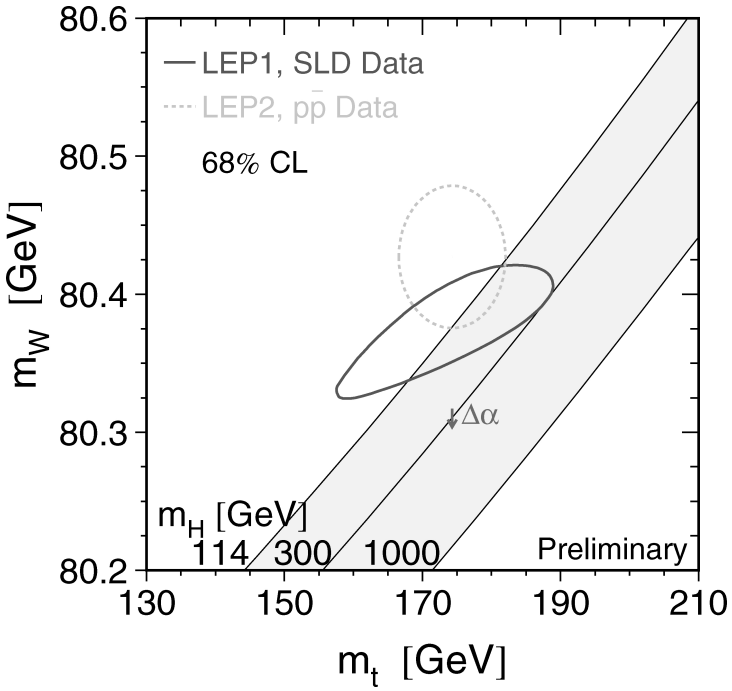

Figure 1 The closed curves represent direct (dotted curve) and indirect (solid curve) experimental measurements of M_W and m_t that constrain the standard-model Higgs mass. The shaded band shows the allowed combinations of M_W and m_t for different values of M_H.

16 Jul 2003 16:50 AR AR199-NS53-09.tex AR199-NS53-09.sgm LaTeX2e(2002/01/18) P1: IKH

experimentally constrained to be heavier than all other known fermions, but some may yet be lighter than the top quark and can appear on-shell in its decays. The top-quark mass is also very close to the energy scale of electroweak symmetry breaking. Indeed, top's Yukawa coupling to the Higgs boson is curiously close to 1. The apparently special value of the top mass raises the possibility that perhaps it has a distinct origin and is not generated by the standard-model Higgs mechanism that is the putative source of other quark and charged-lepton masses.

1.1. Theoretical Perspective

In the standard model, the top quark is defined as the weak isospin partner of the bottom quark. As such, it is a spin-$\frac{1}{2}$ fermion of electric charge $+\frac{2}{3}$ and transforms as a color triplet under the SU(3) gauge group of strong interactions. None of these quantum numbers has yet been directly measured, although a large amount of indirect evidence supports the standard-model assignments. Precision measurements of the $Z \to b\bar{b}$ partial width and forward-backward asymmetry at LEP (16), of B^0-$\bar{B}^0$ mixing, and limits on flavor-changing neutral-current (FCNC) decays of B mesons require the existence of a particle with $T_3 = \frac{1}{2}$, $Q = \frac{2}{3}$, and mass near 170 GeV, consistent with the direct measurements by the Tevatron experiments (17). The Tevatron $t\bar{t}$-production cross-section measurements are also consistent with theoretical calculations for a color-triplet quark. Tevatron Run 2 will make more stringent tests, sufficient to remove any doubt that the Tevatron top is not the standard-model top quark, but direct measurement of some of the top-quark quantum numbers will be possible only at the LHC and a linear collider.

The most pressing challenge in particle theory is to explain the dynamics behind mass generation, which has two aspects: electroweak symmetry breaking (EWSB), whereby the W and Z bosons acquire mass; and flavor symmetry breaking (FSB), which splits the fermions into generations hierarchically arranged by mass. The standard model accommodates both by postulating a fundamental scalar field, the Higgs boson. But a fundamental scalar does not by itself satisfactorily explain the dynamics, and the Higgs sector runs into problems at high energy scales. One well-studied new-physics explanation for this is technicolor (TC), which postulates a new strong gauge interaction at the TeV scale. The top quark often plays a central role in this class of models. Another possibility is supersymmetry (SUSY), a new global spacetime symmetry. The minimal supersymmetric standard model (MSSM) assigns a bosonic (fermionic) superpartner to every fermion (boson) in the standard model and predicts that the lightest superfermion (sfermion) masses are close to those of their standard-model partners. The large top-quark mass usually plays a central role in hiding the electroweak symmetry in supersymmetric models. Direct searches at LEP and the Tevatron have set lower limits on the masses of various SUSY particles (16). All of these are well above m_b, but there is still enough room for SUSY decays of the top quark. A number of other theories postulate exotic particles and interactions or new spacetime dimensions for diverse reasons, often cosmological. In many of these, its large mass makes the top quark a likely connection to new physics.

1.2. The Experimental Arena

1.2.1. PRODUCING TOP QUARKS To date, only the Tevatron proton-antiproton collider, which operated in Run 1 at $E_{\rm cm} = 1.8$ TeV, has had sufficient energy to produce top quarks. The data collected during its Run 1 amounted to $\sim$600 $t\bar{t}$ pair events produced in each of the detector experiments CDF and DØ. Only a small fraction of these passed the stringent selection criteria imposed at the trigger level to suppress enormous QCD backgrounds. The surviving event samples were sufficient to establish the discovery of the top quark and to allow some initial measurements of its properties, principally mass. The current Run 2, with upgraded detectors and an improved accelerator complex now operating at $E_{\rm cm} = 1.96$ TeV, will result in perhaps a 100-fold increase in $t\bar{t}$ event yield by 2008. This will allow a more detailed examination of the top quark, sufficient to confirm its standard-model character, by drastically improving the Run 1 measurements and making new ones possible.

Scheduled to start operation in 2007, the 14-TeV pp Large Hadron Collider (LHC) is expected to deliver nearly eight million top pair events to each of its two experiments, ATLAS and CMS, in the first year alone. The rate will increase by up to a factor of 10 in subsequent years. Even with a modest acceptance, many rare processes involving the top quark will become accessible. sight

Beyond the LHC, the particle physics community has set its ~~sights~~ on a 500–1000-GeV e^+e^- linear collider. Although the $t\bar{t}$ cross section would be tiny compared to that at the LHC or even the Tevatron, the integrated luminosity of 1000 fb^{-1} would be large enough to produce at least half a million top-pair events in about five years of running. Moreover, such a machine offers two main advantages for precision studies. First, $t\bar{t}$ production is an electroweak process. Theoretical calculations are known to much higher precision in this case, and the absence of enormous QCD backgrounds would yield extremely high-purity samples and nearly fully efficient event collection. Second, because the center-of-mass energy of the colliding beams is known with high precision, top quarks could be reconstructed much more precisely. Tuning the beam energy to scan the production threshold will enable super-precision measurements of mass and width. Control over beam polarization would provide exceptionally detailed determinations of couplings. In short, a linear collider would be an ideal machine for precision top-quark physics. However, the main focus here is on recent or approved experiments, i.e., the hadron colliders Tevatron and LHC. For more details on linear collider potential, the reader is referred to References (18) and (19). Table 1 summarizes some key parameters for the colliders mentioned above.

1.2.2. DETECTING THE TOP QUARK A top quark's production and decay vertices are separated by $O(10^{-16})$ m, a distance smaller by many orders of magnitude than the spatial resolution of any detector. Detection of a top quark therefore proceeds through identification and reconstruction of its daughter particles. Fortunately, its large mass dictates that it is not produced highly relativistically. Consequently, its much lighter decay products have good angular separations and high momenta

in the laboratory frame, the center-of-mass frame of the colliding beams. Most end up in the central region of the detector, with $\vec{p}_T$, the momentum component perpendicular to the beamline, exceeding 20 GeV in magnitude.[1]

Top-decay products span the entire spectrum of quarks and leptons. Within the standard model, the top quark decays almost exclusively into Wb. The W decays almost instantaneously (lifetime $\sim 3 \times 10^{-25}$ s) in one of two ways:

- leptonically, into a lepton-neutrino pair—$B(W \to \ell\nu_\ell) = B(W \to \mu\nu_\mu) = B(W \to \tau\nu_\tau) \approx 1/9$
- hadronically, into two jets through a quark-antiquark pair ($u\bar{d}$, $c\bar{s}$ with equal probabilities)—$B(W \to q_1\bar{q}_2) = \frac{2}{3}$.

Hadronic final states manifest themselves as a shower of particles called a jet. If the W decays leptonically, then the charged lepton can be identified with relative ease (except for tau), whereas neutrinos escape direct detection. Figure 2 shows a graphical representation of the various standard-model branching fractions of top pairs. Normally, in the experimental context of hadron colliders, only electrons and muons are referred to as leptons, since tau final states behave so differently.

This large and complex set of final-state permutations has significant implications for data collection. A multilayered hardware and software triggering system is designed to retain as many of the most interesting events as possible. The detector is almost hermetic, by which we mean that it is built to contain as much of an event's transverse energy as possible. Nevertheless, some fraction of top events will be lost depending on the decay mode and distribution, as well as the priorities of the experimental program. A brief account of the major issues for particles entering the detector is in order:

- Electrons are recognized with about 90% efficiency by their short interaction length, which spawns a compact shower in the calorimeter, and an associated track of matching momentum in the central tracking volume of the detector.
- Muons are highly penetrating particles. They are distinguished by their minimum-ionizing trail all the way through, being the only particles to reach the outermost detector layers, with about 90% efficiency.
- Neutrinos escape direct detection because they interact so feebly. Because the beam-axis component of net event momentum varies over a wide range at a hadron collider, only the transverse component of invisible particles' total momenta, $\vec{p}\!\!\!/_T$ ($\vec{\not{E}}_T$), can be inferred in any given event. Simplistically, it is the negative vector sum of observed particles' transverse momenta. The $\vec{\not{E}}_T$ resolution depends strongly on the content and topology of an event.

[1]Transverse momentum, $\vec{p}_T$, implies momentum measurement with a magnetized tracker (e.g., for electrons and muons), whereas transverse energy, $\vec{E}_T$, implies calorimeter energy measurement (e.g., for jets). The two have the same physical interpretation but different resolutions.

16 Jul 2003 16:50 AR AR199-NS53-09.tex AR199-NS53-09.sgm LaTeX2e(2002/01/18) P1: IKH

- Detecting b quarks is particularly important in selecting top event candidates because most background events do not contain them. A b immediately hadronizes, but typically travels about half a millimeter from the primary interaction vertex before decaying into a jet containing multiple charged particles. Such a displaced decay vertex can be isolated using a good vertex detector by extrapolating the tracks associated with the jet to a common origin (secondary vertex tagging). Jets initiated by gluons and lighter quarks (except sometimes c) are rarely associated with a secondary vertex. Additionally, about 20% of the time a b jet contains a lepton, which typically has a lower momentum than a prompt lepton from a W decay. This offers an alternative means for tagging a b-quark jet (soft lepton tagging). Overall, b quarks can be identified about 60% of the time.
- Tau leptons decay leptonically 36% of the time and hadronically 64%. In addition to two neutrinos, the leptonic decays result in an electron or a muon that are typically softer than those from W decays. Apart from a very small impact parameter that is difficult to measure, $W \to \tau\bar{\nu}_\tau \to \ell\bar{\nu}_\ell\nu_\tau\bar{\nu}_\tau$ ($\ell = e, \mu$) decays cannot really be singled out from $W \to \ell\bar{\nu}_\ell$ in top events and are automatically accounted for in the measurements with electron and muon final states. The hadronic modes need special consideration: ~~76~~% of these yield a single charged daughter (one-prong) and ~~24~~% yield three (three-prong). Good pattern-recognition algorithms can exploit the low charge multiplicity and characteristic features of the associated narrow shower in the calorimeter to separate hadronic tau decays from the copious QCD background. The associated neutrino carries away a significant fraction of the tau momentum. This makes tau reconstruction dependent on the distribution of other objects in the event. Overall, the identification efficiency of hadronic tau decays is about 50%.
- Jets initiated by gluons and lighter quarks have nearly full detection efficiency, although establishing their partonic identity event by event is not possible because they hadronize into overlapping states. Subtle differences in profiles of gluon and quark jets may be discernible on a statistical basis. The distinction would be very useful to top-quark studies, since all jets from top decays are quark-initiated (discounting final-state radiation), whereas jets in the QCD background are predominantly gluon-initiated. This possibility requires further studies in the context of hadron colliders. Jets arising from gluons and lighter quarks will be misidentified as b quarks (τ) at a rate of only about $1/200$. They fake an electron or muon even more rarely, at about the $1/2000$ level.

Top-quark decays are no less varied in scenarios beyond the standard model. Therefore, identification of all of these objects, as well as accurate and precise measurement of their momenta, are key to studies of the top quark. Detailed description of the detector design and performance specifications are available elsewhere (21–23).

16 Jul 2003 16:50 AR AR199-NS53-09.tex AR199-NS53-09.sgm LaTeX2e(2002/01/18) P1: IKH

Detailed comparisons of the experimental measurements of the nature of top-quark production (cross section and kinematics), decay (partial widths, angular correlations among decay products, and so on), and other properties (mass, discrete quantum numbers, etc.), with those theoretically predicted are important probes for new physics. It is a challenge for theorists and experimentalists alike to perform calculations and measurements at the highest possible level of precision. For readers interested in greater detail, especially from an experimenter's point of view, we strongly recommend Reference (24) for the Tevatron and Reference (20) for the LHC. Earlier accounts of the discovery of the top quark can be found in References (25) and (26).

2. TOP-QUARK PRODUCTION

At hadron colliders, two distinct standard-model production mechanisms are possible: dominant $t\bar{t}$ pair production via the strong interaction and single-top production via the electroweak interaction. Detailed comparison between standard-model predictions and experimental measurements of physical observables related to top-quark production is an important probe for new physics.

2.1. Pair Production

In the standard model, $t\bar{t}$ pairs are produced via quark-antiquark ($q\bar{q}$) annihilation and gluon fusion. Figure 3 shows the corresponding leading-order (LO) Feynman diagrams.

The total tree-level (Born approximation) $t\bar{t}$ cross section at hadron colliders is a convolution of the parton distribution functions (PDFs) for the incoming (anti)protons and the cross section for the partonic processes $q\bar{q}, gg \to t\bar{t}$:

$$\sigma\left(s, m_t^2\right) = \sum_{i,j} \int_0^1 dx_1 \int_0^1 dx_2 \, f_i\left(x_i, \mu_f^2\right) \, f_j\left(x_j, \mu_f^2\right) \, \hat{\sigma}_{ij}\left[\hat{s}, m_t, \alpha_s\left(\mu_r^2\right)\right]. \quad 1.$$

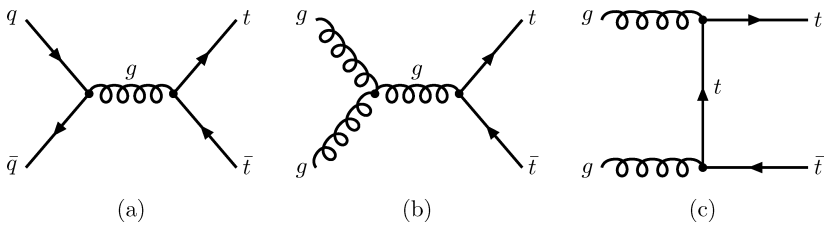

Figure 3 Leading-order Feynman diagrams for strong-interaction production of $t\bar{t}$.

16 Jul 2003 16:50 AR AR199-NS53-09.tex AR199-NS53-09.sgm LaTeX2e(2002/01/18) P1: IKH

Here i, j are the possible combinations of incoming gluon or $q\bar{q}$ pairs and $f(x, \mu_f^2)$ are the PDFs, evaluated at some factorization scale μ_f corresponding to a scale in the problem, such as m_t, and a value x that is the fraction of incoming (anti)proton energy carried by the parton. The partonic subprocess cross sections, integrated over phase space, are functions of the center-of-mass energy $\sqrt{\hat{s}}$, the top-quark mass m_t, and the QCD strong coupling constant α_s evaluated at a renormalization scale μ_r. This scale is also typically taken to be one relevant to the process, e.g., m_t, but it need not be the same as μ_f. At higher orders, the partonic cross section also depends on μ_f, μ_r: $\hat{\sigma}_{ij}[\hat{s}, m_t, \mu_f, \mu_r, \alpha_s(\mu_r^2)]$.

At the Tevatron, $t\bar{t}$ production occurs close to, but not quite at, threshold. The maximum of $d\sigma_{t\bar{t}}/d\hat{s}$ occurs at around 1.5 times the threshold energy, and the average speed of the top quarks is $\beta \approx 0.5$. If for threshold we set $x_i \approx x_j = x_{\rm thr}$, from $\hat{s} = x_i x_j s$ we obtain $x_{\rm thr} \approx 2m_t/\sqrt{s}$. In Tevatron Run 1, $x_{\rm thr} \approx 0.2$, where the quark densities are considerably larger than the gluon densities, $q\bar{q}(gg) \to t\bar{t}$ accounted for 90%(10%) of the cross section.[2] In Run 2, $\sqrt{s} = 1.96$ TeV, the total cross section is about 40% larger, with 85%(15%) coming from an initial $q\bar{q}(gg)$ pair. At the LHC, the situation is reversed: $x_{\rm thr} \sim 0.025$, a regime where gluons dominate, so the $q\bar{q}(gg)$ contributions are about 10%(90%). Table 1 summarizes the $t\bar{t}$ cross sections at the Tevatron, LHC, and a linear collider and compares them to other important standard-model processes. At the Tevatron, roughly one in 10^{10} collisions produces top-quark pairs. In Run 1 the average top production rate was $\sim 5 \cdot 10^{-5}$ Hz, expected to reach $\sim 7 \cdot 10^{-4}$ Hz in Run 2. In comparison, the rate will be about 10 Hz at the LHC, a true top factory.

The uncertainty in $\sigma_{t\bar{t}}^{\rm LO}$ at hadron colliders is large, $\sim$50%. The primary source centers around the scale choices μ_f and μ_r and their effects on α_s. Furthermore, α_s is relatively large, so additional terms in the perturbative expansion for the cross section can be significant. These issues can be addressed by calculating the cross section at next-to-leading order (NLO) in perturbation theory, which we discuss in the next section. Additional, smaller sources of uncertainty are the PDFs and the precise values of m_t and $\alpha_s(M_Z^2)$. At the Tevatron, the cross-section sensitivity due to PDFs is small mainly because the process is driven by the well-measured quark distributions. This is not the case at the LHC, where a $\sim$10% uncertainty in $\sigma_{t\bar{t}}$ comes from the PDF for the dominant gg component.

2.1.1. HIGHER-ORDER CORRECTIONS AND THEORETICAL UNCERTAINTIES At leading order, the $t\bar{t}$ cross section is usually evaluated for $\mu_f = \mu_r = m_t$, since m_t is the only relevant scale in the problem (one could also argue for $2m_t$ for α_s, but $\mu_r = \mu_f$ is the more common choice). Because this is much larger than the scale of QCD confinement, $\Lambda_{\rm QCD} \approx 200$ MeV, the calculation can be trusted to behave perturbatively. But what does the scale choice signify? After all, both PDFs and $\alpha_s(M_Z^2)$ are data extracted from experimentally measured cross sections. However,

[2]For the partonic cross sections, $\sigma_{gg} > \sigma_{q\bar{q}}$, but parton densities are the dominant effect.

16 Jul 2003 16:50 AR AR199-NS53-09.tex AR199-NS53-09.sgm LaTeX2e(2002/01/18) P1: IKH

they are based on processes very different from those we wish to consider at hadron colliders. We have to let α_s run and the PDFs evolve from the scales relevant for extraction to the scales relevant for application. The calculation of the process under consideration is separated into two parts: the perturbative hard scattering (here, $q\bar{q}, gg \to t\bar{t}$) and the perturbatively resummed PDF evolution, which uses nonperturbative input. To this end, the scales μ_r and μ_f are introduced to separate the perturbative and nonperturbative parts of the calculation.

By construction, physical observables in a renormalizable field theory do not depend on a scale. But this is true only to all orders in perturbation theory, which is impossible to calculate. At fixed order, the scale independence is not realized. Higher orders help restore this, removing bit by bit the scale dependence we artificially introduced. Varying the scale at a given order gives one an idea of the residual calculational uncertainty.

In a higher-order calculation, all diagrams that contain the same order in the relevant coupling (here, α_s) must be included. Thus, the full $O(\alpha_s^3)$ NLO calculation (27) includes both real parton emission and virtual (loop-diagram) corrections, even though the different parts do not contain the same number or even type of final-state particles. The NLO corrections increase $\sigma_{t\bar{t}}$ by about 30%, with the uncertainty from varying the scale choice reduced to about 12%.

An important point to note is that the order of the hard-scattering process evaluated must match that of the PDF set used. At each higher order in α_s, there are strong cancellations between terms in the PDF evolution and in the hard-scattering real emission, which come from the artificial dependence on μ_f introduced by factorizing the problem in the first place. For NLO calculations, NLO PDFs must be used; for LO calculations such as parton-shower Monte Carlo, LO PDFs must be used. Noncompliance can introduce large errors.

The NLO calculation of $\sigma_{t\bar{t}}$ experiences large logarithms $\sim\alpha_s \log^2 \beta$, where β is some definition of the threshold dependence (which can vary at NLO), arising from real emission of a soft gluon. As $\beta \to 0$ at threshold, the calculation becomes unstable. Fortunately, real radiation there is restricted by phase space, so soft gluons approximately exponentiate: An $(\alpha_s \log^2 \beta)^n$ term appears at all orders in perturbation theory, with a coefficient at each order of $1/n!$ from permutations over identical gluons, resulting in a series that is simply an exponential containing $\alpha_s \log \beta$. Calculating it is called resumming the large logs. This behavior is a direct consequence of soft-gluon emission in QCD factorizing both in the matrix element and in phase space. A leading-log (LL) resummation takes care of the $(\alpha_s \log^2 \beta)^n$ series, a next-to-leading-log (NLL) resummation the $[\alpha_s(\alpha_s \log^2 \beta)]^n$ series, and so on. This is an overly simplistic picture, but it conveys an idea of what resummation calculations address.

According to one recent NLO + NLL complete resummation calculation (28), with PDF-updated results for the LHC in Section 2 of Reference (20), resummation effects are at the $O(5\%)$ level for both the Tevatron and LHC. Results are $\sigma_{t\bar{t}} = 5.19(6.70)$ pb for $p\bar{p}$ collisions at $\sqrt{s} = 1.8(1.96)$ TeV and 825 pb for pp collisions at 14 TeV, where the uncertainties are from scale variation. Another $\sim$6% contribution comes from PDFs and α_s.

Another recent Tevatron-only study (29) is a partial NNLO + NNLL calculation, in which the exponential expression is expanded to the first three powers of the large logs at $O(\alpha_s)$ and $O(\alpha_s^2)$. This study finds a 5%–20% uncertainty, depending on the $t\bar{t}$ kinematics considered, and averages the results to construct total estimates of $\sigma_{t\bar{t}}$ (1.8 TeV) $= 5.8 \pm 0.4 \pm 0.1$ pb and $\sigma_{t\bar{t}}$ (2.0 TeV) $= 8.0 \pm 0.6 \pm 0.1$ pb, where the first uncertainty is due to kinematics and the second is from scale uncertainty.

The Tevatron results of References (28) and (29) are not necessarily contradictory, since they use different methods that selectively incorporate different higher-order terms. For uncertainties at the LHC, the relation is (20) $\frac{\delta\sigma}{\sigma} \sim 5\frac{\delta m_t}{m_t}$, i.e., if 1 GeV in δm_t is achievable, then the cross section should be known to about 3% experimentally. This makes improvements in $\sigma_{t\bar{t}}^{\mathrm{NLO}}$ desirable, although a complete NNLO calculation is not likely to be completed soon. At the very least, it would be useful to have an improved understanding of PDFs, such as a more sophisticated PDF-uncertainty analysis.

Besides the soft-gluon effects, Coulomb effects may enhance or deplete the cross section near threshold. However, these are found to be negligibly small for $t\bar{t}$ production at both the Tevatron and LHC (30), much smaller than the inherent uncertainty in the NLO + NLL calculations. The same holds true for electroweak corrections, found to be -0.97% to -1.74% of $\sigma_{t\bar{t}}^{\mathrm{LO}}$ for $60 < M_H < 1000$ GeV (31).

2.1.2. EXPERIMENTAL MEASUREMENTS: CROSS SECTIONS, KINEMATICS We now turn to the question of how the $t\bar{t}$ production cross section is measured experimentally and how accurate these measurements are expected to be.

Within the standard model, the top quark decays almost exclusively into a W boson and a b quark. The channels and branching fractions for $t\bar{t}$ decays can be readily derived from those for W decays given in Section 1.2.2. Because of the uniqueness of their experimental detection, channels involving tau leptons are usually treated separately. In the context of object identification in the detector, unless noted otherwise, a "lepton" normally refers to an electron or a muon. Thus, the $t\bar{t}$ final state is categorized as "dilepton" (branching fraction $= 5\%$), "single-lepton (plus jets)" (30%), and "all-hadronic" (44%) depending on whether both, only one, or neither of the two W bosons decay leptonically into an electron or a muon and the corresponding neutrino (Figure 4). The remaining 21% involves tau leptons: 6% for tau-dilepton ($e\tau$, $\mu\tau$, $\tau\tau$) and 15% for τ + jets.

0.05, 0.30, 0.44, to be consistent with p. 332

• **Modeling $t\bar{t}$ production**

Accurate simulation of collision events is critical to understanding how to derive reliable physics measurements from the detector data. Experimentalists use Monte Carlo generators such as PYTHIA (32), HERWIG (33), or ISAJET (34) to model $t\bar{t}$ production in hadron collisions. These include approximate treatments of higher-order perturbative effects (initial- and final-state gluon radiation), hadronization of the final-state partons, the underlying event, and secondary particle decays. The simulations begin by using an exact matrix-element calculation (QCD or electroweak) of the hard-scattering process, such as $q\bar{q} \to t\bar{t}$, then simulate the

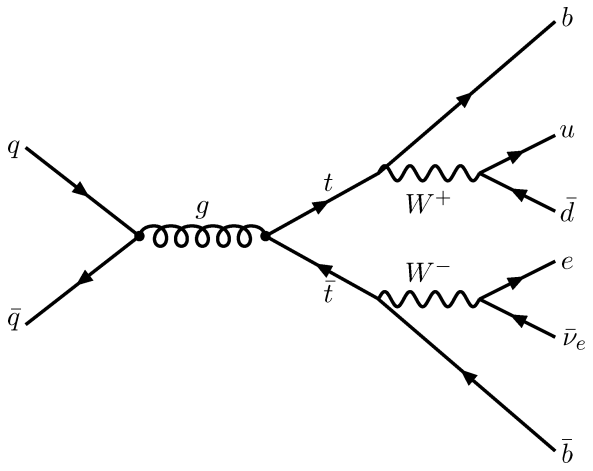

Figure 4 Leading-order Feynman diagram of single-lepton decay of a $t\bar{t}$ event.

emission of additional partons from the incoming and outgoing partons in the hard process. This is done with a parton-shower algorithm that evolves the emitted parton energies downward to a cutoff point, where hadronization takes over.

A more detailed description of these Monte Carlo programs can be found elsewhere (e.g., (20)). The events these generators produce are then combined with the simulation of the detectors' response to the final-state particles. Event-selection cuts can then be studied to understand how best to optimize the signal acceptance while reducing backgrounds from other physics processes that can fake a $t\bar{t}$ signature.

There are small discrepancies between some of the predictions in these Monte Carlo programs. For example, PYTHIA and HERWIG introduce different amounts of gluon radiation (35, 36). Tests comparing distributions from the Monte Carlo predictions to the NLO calculations can be found, for example, in Reference (37), which concludes that in the low-p_T region HERWIG more closely approximates the NLO calculations.

It is clear that as larger $t\bar{t}$ datasets are gathered by the experiments, more detailed comparisons between data and Monte Carlo predictions will be feasible, and a positive-feedback loop will be established. This will improve our understanding of mechanisms behind the more subtle aspects of $t\bar{t}$ production. Accurate modeling will be critical in detecting any possible deviation from the standard-model predictions.

• Event selection and backgrounds

It is important to understand how the rare $t\bar{t}$ events are selected from the flood of other events generated in hadron collisions, and how they are separated from backgrounds that pass the same selection criteria. We discuss the experiments at the Tevatron and then point out the differences, if any, for the LHC.

16 Jul 2003 16:50 AR AR199-NS53-09.tex AR199-NS53-09.sgm LaTeX2e(2002/01/18) P1: IKH

As would be expected in the decay of a massive, slow-moving particle ($\beta \ll 1$) into almost massless ones, the final-state particles in top decay typically carry large transverse momentum in the lab frame ($p_T > 15$–20 GeV) and often go into the more central part of the detector ($|\eta| < \sim 2.5$).[3] Therefore, regardless of channel, the first experimental criterion for detecting top events is high p_T for all decay products. This requirement goes a long way in suppressing backgrounds, especially processes with jets from QCD radiation, which have an exponentially falling E_T spectrum, and processes in which $\not\!\!E_T$ is an artifact of instrumental imprecision, not the escape of real, high-p_T neutrinos.

Other topological cuts, such as requiring that the leptons and $\not\!\!E_T$ are isolated from jet activity and more global event variables such as scalar E_T (H_T, the scalar sum of E_T of all observed objects), sphericity, and aplanarity,[4] help enhance the signal-to-background ratio (S:B). The last two are variables calculated from the eigenvalues of the normalized momentum tensor. Aplanarity ($\mathcal{A}$), proportional to the smallest of the three eigenvalues, measures the relative activity perpendicular to the plane of maximum activity. Sphericity ($\mathcal{S}$), proportional to the sum of the two smaller eigenvalues, measures the relative activity in the plane of minimum activity. Top-quark events typically have larger values of H_T, $\mathcal{S}$, and $\mathcal{A}$.

Finally, the b-tagging requirement eliminates most non-top QCD contamination of the signal, reducing it by about 100-fold, compared to $\sim$75% of the top events yielding at least one tagged b-jet.[5] Tagging heavy-flavor jets with soft leptons helps disentangle systematic uncertainties of the QCD heavy-flavor content.

Remaining backgrounds in the all-hadronic channel arise mainly from QCD multijet production, in which b tags from real heavy-flavor quarks (mostly b, but also some c) or from fakes (gluons or light quarks) are present. The S:B ranges from 1:5 to 1:1 depending on details of the selection. In the single-lepton channel, the most copious background is from $W +$ jets events before b tagging and from $W +$ heavy-flavor after. The S:B after b tagging is typically between 1:1 and 4:1, again depending on the exact criteria. For dileptons, S:$B \approx 1$:2, even without b tagging, with backgrounds coming mainly from WW, $Z \to \tau^+\tau^-$, and dilepton production, all with additional jets from QCD radiation. The background in this case becomes negligible if the requirement of b tagging is added. This is because these backgrounds are all either electroweak-suppressed or arise only from several small branching fractions successively. Including branching fractions and efficiencies of the full chain of selection criteria, only a few percent of the $t\bar{t}$ events produced in the collisions end up in the final sample. In Run 1, an estimated 5% made it to the all-hadronic candidate pool, about 5% to the single-lepton pool, and only about 1% to the dilepton pool.

[3] $\eta = \frac{1}{2} \ln \frac{E+p_z}{E-p_z}$ is called the pseudorapidity, which for massless particles is $\eta = -\ln(\tan \frac{\theta}{2})$.
[4] These terms are defined in, e.g., Reference (38).
[5] The efficiencies of Section 1.2.2 are moderated by the fiducial acceptance of the detector.

16 Jul 2003 16:50 AR AR199-NS53-09.tex AR199-NS53-09.sgm LaTeX2e(2002/01/18) P1: IKH

without (with)?

An excess of about 10 dilepton events over an expected background of four events was observed in the combined data samples of CDF and DØ. It has been suggested that some of these candidates have unusual kinematics (39); Run 2 should resolve this question. In the single-lepton channel, ~~with (without)~~ b tags, an excess of about 60 (10) events was observed over an expected background of about 40 (9). In the all-jet channel DØ (CDF) observed an excess of 16 (43) events over a background of about 25 (144).

At the LHC, very pure signals should be obtained in the dilepton and single-lepton channels. For 10 fb^{-1}, with selection criteria similar to those used at the Tevatron, about 60,000 b-tagged dilepton events are expected, with $S{:}B \approx 50$ (20). In the single-lepton channel, the yield will be close to one million b-tagged events. Because the QCD cross section for $W +$ jets grows more slowly with collision energy than does $t\bar{t}$, $S{:}B \approx 20$ should be possible. However, extracting such a clean signal in the all-jets channel out of overwhelming QCD background is not deemed feasible. Ongoing studies selecting on more sophisticated kinematical variables and using multivariate discriminants show a paltry $S{:}B \approx 1{:}6$.

Figure 5 shows the $t\bar{t}$ cross-section results individually from CDF and DØ in Run 1 for the different decay channels, and the combined results (2). The measurements, within their ~30% uncertainties (dominated by the statistical component), are consistent with standard-model predictions. In Run 2, a precision of 10% is believed achievable with only 1 fb^{-1} of data. Many other factors will then limit the measurement, mostly from calculation of the total acceptance (lepton and b-tagging efficiencies, event-generator systematics, jet energy scale, and luminosity-measurement uncertainty, among others). Prospects for reducing these various components are addressed as needed in Section 4.

2.2. Single-Top Production

Single-top-quark production cannot occur in flavor-conserving QCD, so it probes the charged-current weak interaction connecting top to the down-type quarks, with amplitudes proportional to the quark-mixing matrix element V_{tq} ($q = d, s, b$). This interaction has a vector-minus-axial-vector ($V - A$) structure because only the left-chiral component of fermions participates in the SU(2) gauge interaction. Also because of the weak interaction, single top quarks are produced with nearly 100% polarization, which serves as a test of the $V - A$ structure.

Figure 6 shows the three different ways a hadron collision can produce top quarks singly. The process $q\bar{q} \rightarrow t\bar{b}$ via a virtual s-channel W boson probes the top quark with a timelike W boson, $q^2 > (m_t + m_b)^2$, whereas the W-gluon fusion (t-channel) processes involve a spacelike W boson, $q^2 < 0$. These production mechanisms are thus complementary, as they probe the charged-current interaction in different q^2 regions. In the third process, associated production, a real W is produced in association with the top quark.

The cross sections for all three processes are proportional to $|V_{tb}|^2$. Therefore, measuring the single top-quark production cross section provides a direct probe

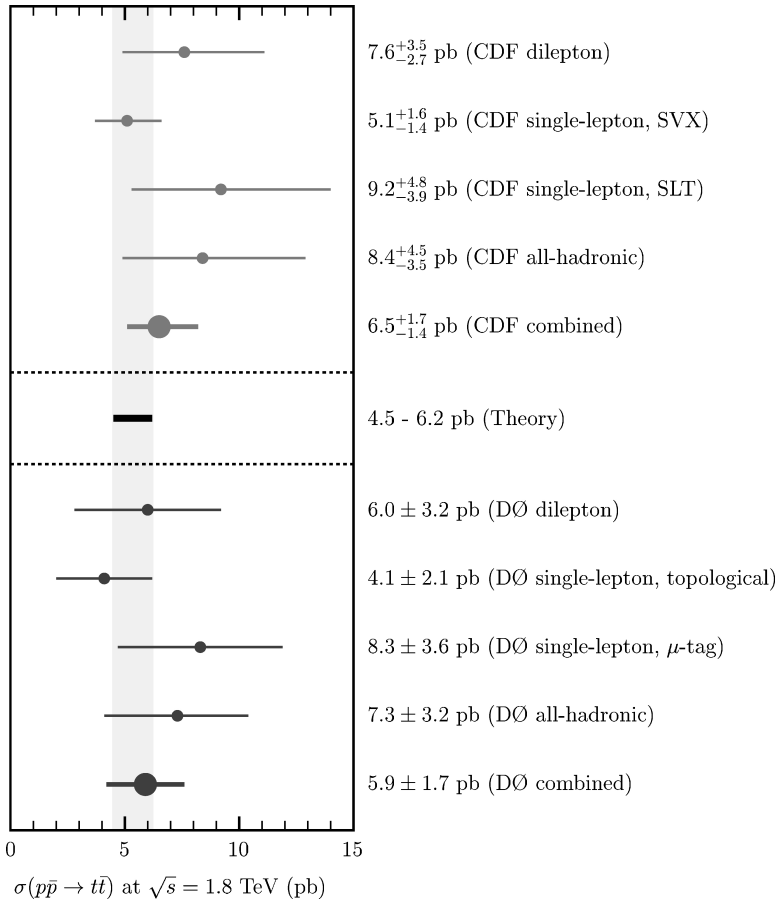

Figure 5 CDF and DØ cross-section results for $t\bar{t}$ production at the Fermilab Tevatron, Run 1, overlaid with the theory prediction. For the latter, we take the entire band covered by both the NLO + NLL and partial NNLO + NNLL predictions (see text).

of $|V_{tb}|$ and the weak tbW vertex in general (we discuss V_{tb} in detail in Section 4.5). Each process can be affected by new physics in a different way. It is therefore important to observe and study each process separately, to the extent allowed by the overlap of the signatures. Studies show that the s- and t channels should be observed at the Tevatron in Run 2 with a data sample of only a few fb^{-1}. The tW-associated production process, however, is smaller in the standard model and will be observed only at the LHC. As we shall see, observing a single top quark is even more challenging than observing $t\bar{t}$. Not only are the cross sections smaller, but the final-state signatures suffer from larger background due to the less distinctive topology of fewer high-p_T jets, leptons, b quarks, and $\not\!\!E_T$.

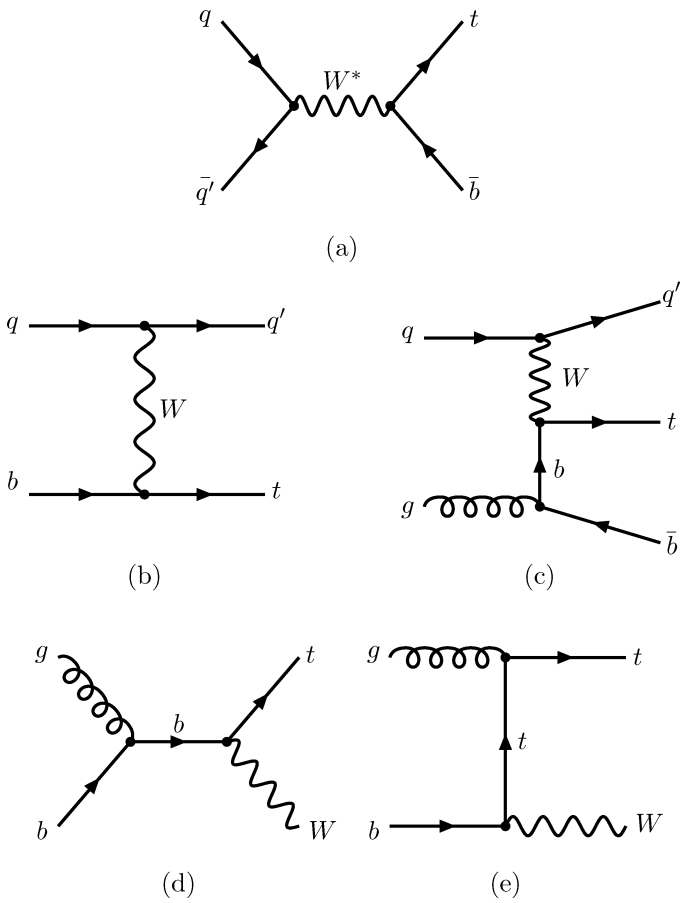

Figure 6 Leading-order Feynman diagrams for electroweak production of single top quarks: (*a*) *s* channel, (*b*, *c*) *t* channel, and (*d*, *e*) associated production with a *W*.

It is interesting to note that $p\bar{p} \rightarrow t\bar{b} \rightarrow Wb\bar{b}$ is a significant background to the standard-model Higgs search channel $p\bar{p} \rightarrow W^+H$; $H \rightarrow b\bar{b}$. Top quarks, produced either singly or in pairs, will generally be a background to a host of other channels of possible new physics. So even if we are satisfied that top has standard-model properties, we must strive for exacting precision in modeling top production for the sake of searches for new phenomena.

2.2.1. SINGLE-TOP PRODUCTION IN THE *S* CHANNEL Figure 6*a* shows the purely electroweak *s*-channel single-top process. Because this arises mostly from initial-state light quarks, where the PDFs are well-known, the hadronic cross section has relatively small PDF uncertainty. The NLO calculations (41–43) show that, for both

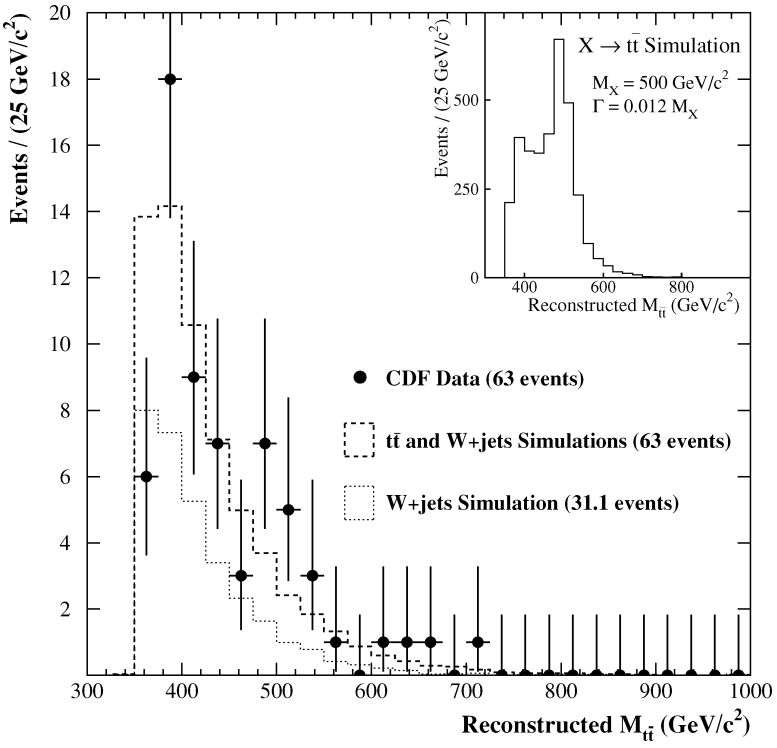

Figure 7 The reconstructed $m_{t\bar{t}}$ distribution in the Run 1 data from the CDF experiment (65).

the Tevatron and the LHC, there is only a relatively small residual dependence on the scales μ_f and μ_r, about $\pm 2\%$. Resummation effects are small, of the order of 3% (42), and Yukawa corrections (loops involving the Higgs-sector fields) are negligible (<1%) at both colliders. The cross section does change, however, by about $\mp 10\%$ at both the Tevatron and LHC if m_t is varied by ± 5 GeV. Thus, 1–2-GeV precision in m_t would be desirable to avoid increasing the theoretical uncertainty further. Because the cross section is potentially so precisely known, this channel may provide the best direct measurement of $|V_{tb}|$ at the Tevatron (see Section 4.5).

In Run 1, the cross section was predicted to be about 0.70 ± 0.04 pb. This is roughly eight times smaller than $\sigma_{t\bar{t}}$, and suffers from comparatively larger backgrounds. An increase of only about 30% is expected in Run 2, whereas an additional factor of 24 is expected for the LHC. Table 2 shows the results of the fully differential NLO calculations (43). Despite the small cross section, as we discuss below, both CDF and DØ started the search for single top quarks back in Run 1, both to establish the technique that will bear fruit in Run 2 and on the chance that new physics increases this cross section greatly beyond standard-model expectations.

TABLE 2 Single top-quark production cross sections (pb)

Process	Tevatron Run 1	Tevatron Run 2	LHC (t)	LHC ($\bar{t}$)
$\sigma^{\mathrm{NLO}}_{s-\mathrm{chan}}$	0.380 ± 0.002	0.447 ± 0.002	6.55 ± 0.03	4.07 ± 0.02
$\sigma^{\mathrm{NLO}}_{t-\mathrm{chan}}$	0.702 ± 0.003	0.959 ± 0.002	152.6 ± 0.6	90.0 ± 0.5
$\sigma^{\mathrm{LL}}_{\mathrm{assoc}}$	—	0.093 ± 0.024	31^{+8}_{-2}	31^{+8}_{-2}

2.2.2. SINGLE-TOP PRODUCTION IN THE t CHANNEL The W-gluon-fusion cross section is illustrated by the Feynman diagrams in Figures 6*b*, *c*. These diagrams are closely related: diagram (*b*) shows the hard matrix element to calculate when the initial parton is treated with a b-quark density (b in the proton sea arises from splitting of virtual gluons into nearly collinear $b\bar{b}$ pairs); diagram (*c*) is relevant if the initial parton is treated as a gluon, and the extra final-state b quark is typically required to appear at large (experimentally observable) p_T. The calculation is less precise than for the s channel because it involves gluon or b-quark PDFs, which have relatively large uncertainties. In general, the inclusive cross section with resummed logarithms predicts the total single-top rate more precisely. On the other hand, an exclusive calculation using gluon densities and a finite-p_t "incoming" b quark might in some cases give better kinematic distributions. Recent literature (44) has highlighted this and corrected some improper uses of b-parton densities in the context of Higgs-boson production. In that context, some factorization-scale issues have proved important, which eventually must be applied to the single-top case.

The final state in this channel is Wbq, with an occasional additional $\bar{b}$ antiquark: $\sim$75% of the total cross section occurs for $p_T(\bar{b}) < 20$ GeV (45), too low to be observed. Absence of the additional b jet helps differentiate this process from the s channel, but the primary distinction is the additional light-quark jet. This is typically emitted at large rapidity, very forward in the detector, where most hard QCD events do not emit jets. This is sometimes known as a forward-tagged jet.

This channel benefits from a larger production rate compared to the s channel. At the Tevatron it is about a factor of three larger, whereas at the LHC it is about a factor of 23 larger. The NLO cross section (46–48) retains a somewhat larger scale dependence than in the s-channel case, about 5% at both the Tevatron and the LHC, but this is still quite good. If the top-quark mass is changed by ± 5 GeV, the cross section changes by about $\mp 8\%(\mp 3\%)$ at the Tevatron (LHC), so its dependence on m_t is comparatively smaller and is probably not the limiting theoretical uncertainty. The Yukawa corrections are also small, $\approx$1%. Table 2 lists the fully differential NLO cross sections for the Tevatron and LHC (43).

2.2.3. ASSOCIATED PRODUCTION CHANNEL Associated production of a single top quark, tW, shown in Figures 6*d*, *e*, proceeds via an initial gb pair, which makes the cross section negligible at the Tevatron. However, at the LHC, associated production contributes about 20% of the total single-top cross section. As in the

t-channel case, one of the initial partons is a b quark. However, unlike the t channel, the rate of this process scales as $1/s$. This, combined with the higher x values needed to produce a top and a W and correspondingly lower quark-parton densities, leads to a cross section about five times smaller than that of the t channel, even though associated production is of order $\alpha_s\alpha_W$ rather than α_W^2 (the ratio of strengths is $\alpha_s/\alpha_W \approx 10$). This cross section has been calculated only at leading order, with a subset of the NLO calculations included (49); its relative unimportance probably makes a full NLO calculation unnecessary. The cross-section uncertainty is ≈10% from PDFs and ≈15% from scale variations. The cross section at the LHC in the standard model is 62 pb with a total uncertainty of ≈30% (see also Table 2).

2.2.4. EXPERIMENTAL STATUS AND PROSPECTS Combining the s- and t-channel cross sections, the total single-top production rate is about 40% of $\sigma_{t\bar{t}}$ at both the Tevatron and LHC. Observing singly produced top quarks is more difficult than observing those pair-produced because the final state of single-top events is less rich in particle content and pole structure. Experimental searches for a single top quark have to take into account subtle kinematical differences between the relatively larger backgrounds and the various single-top production channels. In all cases, at least one W boson and one b jet are present in the final state. To suppress backgrounds from QCD, one is forced to focus on the leptonic W-decay subchannels and on b-tagged events. Therefore, the starting sample for these searches requires a single high-p_T isolated lepton, large $\not\!\!E_T$, and a b-tagged jet. The challenge is to understand very precisely the rate and kinematics of all processes that contribute to the "$W + b +$ jets sample." Only with such understanding, and with enough data that a statistically significant signal can be extracted, can one make a credible claim of single-top observation. We now briefly discuss the searches performed at the Tevatron in Run 1 and the prospects for Run 2 and the LHC.

2.2.4.1. Run 1 searches The CDF and DØ experiments have searched for each of the potentially accessible s- and t-channel signatures separately, and CDF has also performed a combined search. The combined search looked for single top quarks in the $W +$ jets sample, with the W decaying leptonically into an electron or a muon and allowing up to three jets. The (combined) invariant mass of the lepton, $\not\!\!p_T$, and highest-p_T jet must lie between 140 and 210 GeV, bracketing the top-quark mass. This selection was followed by a likelihood fit to H_T, the scalar-p_T sum of all final-state objects seen in the detector. This distribution is on average softer for non-top QCD backgrounds and harder for $t\bar{t}$ production, with single-top production falling somewhere between. The limit extracted by this technique is $\sigma(p\bar{p} \to t + X) < 14$ pb at 95% CL (11).

For the search that separates s- from t-channel production, CDF took advantage of b tagging using displaced vertices and exploited the fact that usually only one b-tagged jet can be expected in the t-channel case. This is because the $\bar{b}$ tends to be collinear with the initial gluon, so that its transverse momentum is too low to be observed. The single- and double-tagged events in the $W + 2$-jet samples were

16 Jul 2003 16:50 AR AR199-NS53-09.tex AR199-NS53-09.sgm LaTeX2e(2002/01/18) P1: IKH

reconstructed separately and subjected to a likelihood fit. The resulting limits (11) are $\sigma_{s-\text{chan}} < 18$ pb and $\sigma_{t-\text{chan}} < 13$ pb.

The DØ experiment used a neural network trained differently for the different channels, and considered tagged and untagged events (tagging for DØ was done by associating nonisolated soft muons with semileptonic b decays). The limits obtained are (12) $\sigma_{s-\text{chan}} < 17$ pb and $\sigma_{t-\text{chan}} < 22$ pb. These limits are about an order of magnitude above the expected standard-model values (see Table 2) but are still useful to establish technique and to rule out major deviations due to new physics.

The backgrounds in these searches arose mainly from $W +$ jets, QCD multijets, and $t\bar{t}$, with a S:B ratio in the range of 1:10 to 1:25, depending on the channel and the strictness of event selection. It proved crucial to use b tagging to reduce the background from QCD multijets (only fakes remained) and from $W +$ jets (principally only $W +$ heavy-flavor remained).

2.2.4.2. Run 2 and LHC plans Experiments in the Tevatron's Run 2 and at the LHC will emphasize the slight differences in kinematic distributions between the various signal and background processes to extract the signal in each of the three channels. Useful variables include jet multiplicity, event invariant mass, reconstructed top invariant mass, invariant mass of all jets, E_T of the jets (including forward jets), H_T, and others. Sophisticated pattern-recognition techniques, such as neural networks with these or similar inputs, will play a large role. Such techniques are now being perfected in order to conduct these searches with better precison.

The Run 2 experiments should be able to achieve 20%–30% precision for the s- and t-channel cross section with 2 fb^{-1}. At the LHC, the t channel, which has the highest yield of the three, is expected to give the most precise cross section and thus the best $|V_{tb}|$ measurement. A S:B of about 2:3 should be reached, with statistical uncertainty of 1%–2%. For the s channel at the LHC, requiring two high-p_T b-tagged jets and no other jets in the event yields S:$B \approx$ 1:12 and statistical uncertainty of about 6%. For the associated production channel (accessible only at the LHC) to maximize signal significance, hadronic decays of the W may be included in the search by constraining a two-jet invariant mass to be close to M_W. This requirement, together with the higher jet multiplicity in the event, helps reduce backgrounds. Simulations predict S:$B \approx$ 1:4 and statistical uncertainty of about 4%.

It is not easy to estimate firmly the systematic uncertainties in these measurements. Luminosity alone can contribute at the level of 5% or more. Further work on this issue must build on experience gained at the Tevatron.

2.3. Sensitivity to New Physics

Top-quark production at hadron colliders, be it $t\bar{t}$ or single-top, is an ideal place to look for new physics. If any new physics is associated with the generation of mass, it may be more apparent in the top-quark sector than with any of the lighter fermions. Many models predict new particles or interactions that couple preferentially to the

third generation and in particular to the top quark. These models extend the strong, hypercharge, or weak interactions in such a way that the new groups spontaneously break into their standard-model subgroup at some scale: $SU(3)_h \times SU(3)_l \rightarrow SU(3)_C$, $SU(2)_h \times SU(2)_l \rightarrow SU(2)_W$, and $U(1)_h \times U(1)_l \rightarrow U(1)_Y$, where h represents the third (heavy) generation and l the first two (light) generations. As a result, one would expect production rate and kinematic distributions of the decay products to differ from the standard-model predictions.

Here we highlight only a few scenarios to illustrate the rich ways that physics beyond the standard model can affect top production. Along the way, we refer the reader to key papers in the vast literature on this subject.

2.3.1. TOP PAIR PRODUCTION In $t\bar{t}$ production, it is especially interesting to study the invariant-mass distribution of the top pair, $d\sigma/dm_{t\bar{t}}$, because it can reveal resonant production mechanisms. Other interesting kinematical distributions are the angle of the top quark with respect to the proton direction (Tevatron only) in the center-of-mass system (50), and the top-quark and W-boson p_T spectra. A partial list of new phenomena that can contribute to the cross-section enhancements and to the distortion of the standard-model kinematical distributions can be found elsewhere (50–57).

One potential source of new physics in $t\bar{t}$ production is supersymmetric corrections to QCD (40). The conclusion is that aside from special regions in MSSM parameter space, the contribution is at most a few percent correction to the total $t\bar{t}$ rate or the $m_{t\bar{t}}$ spectrum, so it is very difficult to infer SUSY this way.

In another scenario, if the top quark is composite, then there would be effects modifying the cross section, depending on the properties of the constituents of the top quark. If these carry color, scattering proceeds through gluon exchange (58, 59). If the light quarks are also composite, then $q\bar{q} \rightarrow t\bar{t}$ can proceed directly through the underlying composite interactions, as well as by QCD gluon exchange (60). In either case, compositeness would result in an enhancement of the $t\bar{t}$ cross section over the standard-model value, which could manifest itself as an enhancement in $d\sigma/dm_{t\bar{t}}$ at large $m_{t\bar{t}}$.

Many theories postulate heavy resonances decaying to $t\bar{t}$, such as technimesons in technicolor models (51, 61) (e.g., $gg \rightarrow \eta_T \rightarrow t\bar{t}$) or other models of strong EWSB (52, 54). Variants of technicolor theories, such as topcolor (62, 63) and topcolor-assisted technicolor (TC2) (63), hypothesize new interactions, mediated, for example, by top-gluons or new weak bosons that are specifically associated with the top quark and that give rise to heavy states: $q\bar{q} \rightarrow g_t \rightarrow t\bar{t}, q\bar{q} \rightarrow Z' \rightarrow t\bar{t}$, etc. Because $t\bar{t}$ production at the LHC is dominated by gg fusion, color octet resonances ("colorons") could also be produced (64). More recently, ~~extradimensional~~ theories propose scenarios in which new scalar bosons couple preferentially to the third generation. Some scenarios in which only these bosons live in the extra dimensions predict particles very similar to the topcolor Z' (57).

Top-quark pair production can be thought of as the modern-day Drell-Yan (dilepton production) process, probing the ultra-heavy intermediate states

predicted by various models. Present and future experiments should patiently scan the $m_{t\bar{t}}$ spectrum for surprises. CDF and DØ have already in Run 1 searched for narrow vector resonances in $m_{t\bar{t}}$ in the single-lepton channel. Within the limited statistics of these samples (63 events, with $S{:}B \approx 1{:}1$ for CDF), no significant peaks were observed. Even though the searches were in principle model-independent, limits on specific models can be extracted. CDF finds that the existence of a leptophobic Z' in a ~~TC2~~ model with mass <480 GeV (<780 GeV) can be excluded at 95% CL if its width is 1.2%(4%) of its mass (65, 66). The DØ search excludes $M_{Z'} < 560\,\text{GeV}$ at 95% CL for $\Gamma_{Z'} = 0.012 M_{Z'}$ (67). These searches will continue in Run 2, extending limits considerably or perhaps revealing something interesting.

Many other kinematical distributions in the top-quark samples were examined in Run 1 (24, 68), testing consistency with standard-model expectations (see e.g., 36, 37, 50). Within the limited statistics of the samples, no significant deviations from the standard model have yet been observed. Nonetheless, some intriguing features, such as large $\vec{\not{E}}_T$ and large lepton p_T, have been noticed in the dilepton samples (39). These could conceivably be attributed to SUSY production. However, multivariable consistency checks do not show overall significant deviations (CDF, private communication). Other samples that overlap with top, such as the CDF b-tagged $W+$ jets sample, show very interesting features, with certain subsamples containing soft-lepton tags that deviate slightly from standard-model expectations. Run 2 data will help determine whether these are statistical fluctuations or whether some new physics is hiding in the data.

The LHC could, of course, discover particles with masses larger than those accessible at the Tevatron. Studies for the ATLAS experiment show 5σ discovery-potential curves for ($\sigma \cdot \mathcal{B}$) versus $m_{t\bar{t}}$ for a hypothetical narrow resonance (20). Particles as massive as 2 TeV could be discovered with datasets of 300 fb^{-1} if $\sigma \cdot \mathcal{B} > 50$ fb.

2.3.2. SINGLE-TOP PRODUCTION Single-top production could also be influenced by new physics through (*a*) unconventional weak interactions (48, 69–72), (*b*) virtual effects of new particles (64, 73–76), or (*c*) new mechanisms that produce single-top-quark events (48, 64, 77–81).

Resonances can also appear in single-top production. For example, a new heavy vector boson $W'^{\pm}$ or charged scalar $\phi^{\pm}$, new SU(2) structure, or extra dimensions can all contribute additional diagrams analogous to those in Figure 6 that affect the rates and kinematics differently. The *s*-channel process would be particularly sensitive to these states, but the *t*- and associated production channels are not expected to be affected significantly (48). Charged scalars feature in models with more than one Higgs doublet, such as the MSSM, and in topcolor models. Processes such as $c\bar{b} \to \pi_t^+ \to t\bar{b}$ contribute significantly to the *s*-channel rate (a factor-of-two enhancement is possible at the Tevatron and even more at the LHC). On the other hand, flavor-changing neutral currents (e.g., a Ztc vertex) would be difficult to see in the *s* channel, whereas the *t* channel would exhibit large effects (48). It has been shown that the *t*-*c*-*g* coupling can be greatly enhanced by introducing

an operator of dimension 5 to the QCD Lagrangian without violating the local strong and (broken) electroweak gauge symmetries (80, 81). Limits can be set on the scale of this new interaction by searching for single-top production via strong-interaction processes, such as $q\bar{q}, gg \to t\bar{t}c$ at the Tevatron and the LHC. Searches for $t\bar{t} \to cgWb$ will yield ~~much~~ weaker limits owing to large background.

Regardless of the specific search for new physics in top-quark production, one must be careful, when studying kinematical distributions, to optimize event selection to detect pure standard-model production that may dilute the effects of new physics. For example, a resonance in $t\bar{t}$ production may distort the summed E_T and sphericity or aplanarity distributions of candidate events from their standard-model expectation (50).

3. TOP-QUARK DECAYS

The standard model predicts $B(t \to bW) > 0.998$. Other decays allowed in the standard model are not only rare but also mostly too difficult to disentangle from backgrounds to be observed in the foreseeable future. Nevertheless, one must try to be sensitive to all conceivable signatures of top-quark decay because some can be enhanced by several orders of magnitude in scenarios beyond the standard model, and these may fall within the LHC's reach. We first review the standard-model decays, then discuss possibilities in the presence of new physics.

3.1. Standard-Model Top-Quark Decays

After $t \to bW$,[6] the next most likely modes are the off-diagonal CKM decays $t \to Ws, Wd$. Along with $t \to WbZ$, these are the only decays allowed at tree level in the standard model; they are discussed in Section 3.1.1.[7] Flavor-changing neutral-current (FCNC) decays, $t \to X^0 q$, where $X^0 = g, \gamma, Z, H$ and $q = c, u$, are loop-induced and highly suppressed by the GIM mechanism (82). Branching fractions are typically $O(10^{-13})$. We discuss these in Section 3.1.2.

3.1.1. CHARGED-CURRENT DECAYS In the standard model, $t \to Wb$ is described purely by the universal $V - A$ charged-current interaction. The W boson is a real particle in top decays, so its helicity is very different than in the decays of any other quark, where the W is highly virtual. The amplitude for a positive-helicity W^+ boson is suppressed by a chiral factor m_b^2/M_W^2, so the W helicity is a superposition of only the zero- and negative-helicity states. At tree level in the standard model,

[6]Henceforth, we do not specify flavor or antiflavor whenever the symmetry is obvious. All statements are equally valid under charge conjugation.

[7]The radiative decays $t \to Wbg$ and $t \to Wb\gamma$ are common, but do not offer any fundamental new insight, unless the branching fractions turn out to be significantly different from the standard-model predictions (0.3 and 3.5×10^{-3}, respectively, for $E_{g,\gamma} > 10$ GeV at the LHC). These channels are generally treated inclusively with $t \to Wb$.

the fraction $\mathcal{F}_0$ of longitudinal (zero-helicity) W bosons in the top rest frame is (83, 84):

$$\mathcal{F}_0 = \frac{m_t^2/M_W^2}{1 + m_t^2/M_W^2} = 0.701 \pm 0.016 \qquad 2.$$

for $m_t \gg M_W$. The large top-quark mass exposes the longitudinal mode of the W, so precise measurement of $\mathcal{F}_0$ serves as a stringent test of the standard model. To this end, CDF analyzed the lepton p_T spectrum in $t\bar{t}$ single-lepton final states in Tevatron Run 1, assuming a pure $V - A$ coupling. They obtained $\mathcal{F}_0 = 0.91 \pm 0.37\,(\text{stat.}) \pm 0.13(\text{syst.})$, consistent with the standard model (16, 85). The statistical uncertainty will be reduced by an order of magnitude in Run 2, and to a negligible level at the LHC. Improvement in the systematic uncertainty has yet to be estimated but should be better than a factor of two.

Such variables as the angle between the lepton and its parent W direction in the top rest frame depend on the W helicity. The invariant mass distribution of the lepton and the b quark in leptonic top-decay candidates, $M_{\ell b}$, can therefore be used to estimate the relative W-helicity fractions and thus the $V + A$ component in top decay. CDF's Run 1 analysis gives $f(V + A) = -0.21^{+0.42}_{-0.25}(\text{stat.}) \pm 0.21(\text{syst.})$ (preliminary) (86), consistent with zero.

The "radiative" decay $t \to WbZ$ has been suggested (87) as a sensitive probe of the top-quark mass, since the measured value of m_t makes this decay close to threshold. The branching fraction varies by about a factor of three within the current experimental uncertainty of $\sim$5 GeV on m_t, but it is in the range $O(10^{-7}$–$10^{-6})$, well beyond the sensitivity of the LHC or a linear collider.

3.1.2. NEUTRAL-CURRENT DECAYS With current experimental input, the standard model predicts $B(t \to cg) \sim 4 \times 10^{-13}$, $B(t \to c\gamma) \sim 5 \times 10^{-13}$, and $B(t \to cZ) \sim 1 \times 10^{-13}$ (88). Although $B(t \to cH^0)$ depends on the Higgs-boson mass, M_{H^0}, it also cannot exceed $\sim 10^{-13}$. These are all well below the detection limits of even the LHC or a linear collider (89). Direct searches for FCNC decays by CDF set limits of $B(t \to c\gamma) + B(t \to u\gamma) < 0.032$ and $B(t \to cZ) + B(t \to uZ) < 0.33$ at 95% CL (15). These limits are dominated by statistical uncertainties and are expected to improve by up to a factor of 10 following Tevatron Run 2. The LHC experiments have also estimated their 5σ discovery reach for these processes. Given a 100 fb^{-1} data sample, the minimum branching fractions accessible to ATLAS and CMS are in the vicinity of 2×10^{-4} for both $t \to Zq$ and $t \to \gamma q$ (20).

Rates are smaller still for $t \to cX_i^0 X_j^0$, where X_i^0, X_j^0 can be any neutral bosons. Such FCNC decays can be significantly enhanced, however, in various scenarios beyond the standard model.

3.2. Top-Quark Decays Beyond the Standard Model

Many channels emerge to compete with top-quark standard-model decays in the presence of new physics. Extended Higgs sectors, alternative mechanisms for

EWSB, and mass hierarchies among supersymmetric particles all attach special significance to the top quark. We first consider minimal extensions to the standard-model Higgs sector without invoking any new symmetries. Special implications within the framework of the MSSM are then addressed, along with other scenarios suggested by SUSY. Finally, we examine topcolor-assisted technicolor (TC2) models.

3.2.1. DECAYS WITH AN EXTENDED HIGGS SECTOR The standard-model Higgs sector consists of a single complex scalar doublet. The single, neutral scalar Higgs boson that arises after EWSB does not affect top-quark decays in any measurable way. However, with the addition of a second Higgs doublet come charged Higgs states, $H^{\pm}$. If kinematically allowed, $t \to bH^{\pm}$ can have a significant branching fraction. This is important not merely because a richer Higgs sector is experimentally allowed but because it is in fact required by some of the leading candidates for new physics. The simplest extension is to two complex scalar doublets, generically called two-Higgs doublet models (2HDM). In this case, EWSB results in five physical Higgs bosons: two neutral scalars (h, H), a neutral pseudoscalar (A), and a pair of charged scalars ($H^{\pm}$). Two new parameters enter at tree level, usually taken to be M_A or $M_{H^{\pm}}$ and $\tan\beta \equiv v_2/v_1$, where v_i are the vacuum expectation values of the Higgs fields ϕ_i ($i = 1, 2$). Both charged and neutral Higgs bosons can appear in tree-level top-quark decays, the latter implying FCNCs.

3.2.1.1. Decays to charged Higgs bosons Among a few variants of the (2HDM) is the "Type 2" model, wherein one doublet couples to up-type fermions and the other to down-type. This division is required, for example, in the MSSM (90).

If $M_{H^{\pm}} < m_t - m_b$, then

$$\Gamma(t \to H^+ b) \propto \left(m_t^2 \cot^2\beta + m_b^2 \tan^2\beta\right)\left(m_t^2 + m_b^2 - M_{H^{\pm}}^2\right) + 4m_t^2 m_b^2 \qquad 3.$$

at tree level. For fixed $M_{H^{\pm}}$, this function is symmetric in $\log(\tan\beta)$ about a minimum at $\tan\beta = \sqrt{m_t/m_b}$. For given $\tan\beta$, the partial width decreases as $M_{H^{\pm}}$ increases. If one ignores fermion masses except when they are multiplied or divided by $\tan\beta$, then in the diagonal CKM approximation the fermionic-decay partial widths are given by

$$\Gamma(H^+ \to U\bar{D}) = \frac{N_c g^2 M_{H^+}}{32\pi M_W^2}\left(m_U^2 \cot^2\beta + m_D^2 \tan^2\beta\right), \qquad 4.$$

where U (D) is an up- (down-)–type fermion and $N_c = 1$ (3) for leptons (quarks). With the current experimental lower limit of $M_h > 91.0$ GeV and $M_A > 91.9$ GeV at 95% CL (91), bosonic decays of the charged Higgs boson, $H^{\pm} \to W^{\pm}h$, $W^{\pm}A$, are kinematically suppressed for $M_{H^{\pm}} < m_t - m_b$, but not forbidden owing to finite-width effects.

Thus, for $\tan\beta > 1$, $H^{\pm} \to \tau\nu_{\tau}$ is the dominant decay channel. If $\tan\beta < 1$, the decay depends on $M_{H^{\pm}}$: For $M_H^{\pm} \approx 100$ GeV, $H^{\pm} \to cs$ and $H^{\pm} \to bc$ compete more or less evenly (CKM suppression due to $|V_{cb}| \ll |V_{cs}|$ is offset by the

16 Jul 2003 16:50 AR AR199-NS53-09.tex AR199-NS53-09.sgm LaTeX2e(2002/01/18) P1: IKH

stronger $H^{\pm}$ coupling to b relative to s); but as $M_H^{\pm}$ is increased beyond 120 GeV, weight gradually shifts to $H^{\pm} \to Wbb$ via a virtual top quark. Strategies for $H^{\pm}$ searches therefore depend on $M_{H^{\pm}}$ and $\tan\beta$. Searches for $e^+e^- \to H^+H^-$ at LEP constrain $M_{H^{\pm}} > 78.6$ GeV at 95% CL (92), whereas the CLEO experiment has set a limit of $M_{H^{\pm}} > (244 + 63/(\tan\beta)^{\frac{1}{3}})$ GeV at 95% CL from the inclusive measurement of $b \to s\gamma$ (93).

By itself, an extended Higgs sector does not significantly alter $\sigma_{t\bar{t}}$ at hadron colliders. One looks instead for either the appearance of $t \to H^{\pm}b$ signatures or, indirectly, the disappearance of the standard-model $t \to Wb$ signatures. For the latter, one assumes $B(t \to H^{\pm}b) + B(t \to Wb) = 1$. Both CDF and DØ conducted searches for $t \to H^{\pm}b$ in $p\bar{p} \to t\bar{t}$ events in Run 1 (13, 14). Figure 8 shows the DØ results from their disappearance search along with projections for Run 2.

The direct searches focused on $H^{\pm} \to \tau\nu$. With good tau identification capability, this can yield the strongest results, albeit limited to $\tan\beta > 1$, where the process has a large branching fraction. Combinations of different methods and of data from the two experiments may indeed eventually give stronger constraints. As expected, searches are more difficult in the region around $\tan\beta = \sqrt{m_t/m_b}$, where $t \to bH^{\pm}$ is highly suppressed. Searches for $H^{\pm} \to cs, cb$ are made more challenging

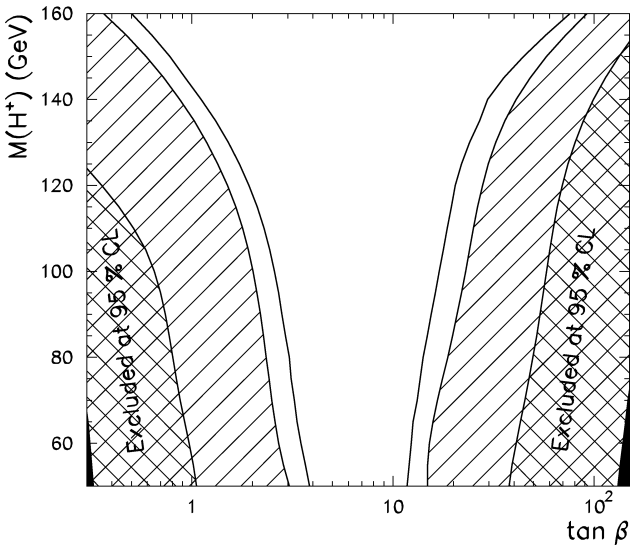

Figure 8 The 95%-CL exclusion boundaries in the $[M_{H^+}, \tan\beta]$ plane from the DØ Run 1 "disappearance search" for $t \to bH^{\pm}$ (double-hatched). Also shown are Run 2 projections if the probability of experimental observations continues to peak at the standard-model prediction: 2 fb^{-1} (single-hatched) and 10 fb^{-1} (unhatched). The modeling is based on leading-order calculations. More recent results from LEP (92) have excluded $M_{H^+} < 78.6$ GeV at 95% CL.

by overlap with the standard-model decay $t \to Wb \to q_1 q_2 b$. However, a dijet invariant-mass peak between 110 GeV and 130 GeV corresponding to $M_{H^\pm}$ is a viable signal for Tevatron Run 2 and the LHC. For $M_{H^\pm} > 130$ GeV, $t \to bH^\pm \to Wbbb$ may offer cleaner signatures, but $B(t \to bH^\pm)$ decreases rapidly with increasing $M_{H^\pm}$. Increased statistics from Run 2 and the LHC will push the exclusion contour wings asymptotically closer (see Figure 8)—or perhaps the process will be observed. The exclusion boundaries in the $[M_{H^\pm}, \tan\beta]$ plane roughly follow contours of constant $B(t \to bH^\pm)$. Thus, 95%-CL upper limits on $B(t \to bH^\pm)$ for $\tan\beta > 1$ (where $H^\pm \to \tau\nu$ dominates) are 0.36 from DØ and 0.5–0.6 from CDF. The disappearance search result from DØ can be interpreted as $B(t \to bH^\pm) < 0.45$ at 95% CL, irrespective of $\tan\beta$ except in the region where $H^\pm \to Wbb$ is the dominant decay mode (i.e., when $\tan\beta < 1$ and $M_{H^\pm} > 125$ GeV). The corresponding estimate for Run 2 is $\mathcal{B}(t \to bH^\pm) < 0.11$ at 95% CL (94).

All $H^\pm$ searches hinge on the fact that, unlike those of $W^\pm$, $H^\pm$ fermion couplings are not flavor-blind. This implies we should compare the values for $\sigma_{t\bar{t}}$ derived from different final states, based on the standard-model assumption of $B(t \to Wb) \approx 1$. For example, if the dilepton, single-lepton, and all-jets $t\bar{t}$ final states exhibited differences, it could indicate significant alternative decay modes to $t \to Wb$. Though less restrictive in assumptions, this method also yields the least stringent conclusions. Tevatron Run 1 data are statistically insufficient for a meaningful application of this method, but that will change for Run 2 and the LHC.

3.2.1.2. FCNC decays in a 2HDM Flavor-changing-neutral-current top-quark decay rates can be enhanced if one abandons the discrete symmetry invoked in the Type 2 2HDM to suppress tree-level scalar FCNCs. In the more general Type 3 2HDM, fermions are allowed to couple simultaneously to more than one scalar doublet (95).[8] Single-vector-boson FCNC decays, $t \to cV_i^0$ ($V_i^0 = \gamma, Z, g$), are still loop-induced, as shown in Figures 9*a*, *b*, but can have branching fractions as large as $O(10^{-5})$ even without any new interactions.[9] Double-vector-boson FCNC decays, $t \to cV_i^0 V_j^0$, also appear at tree level (Figure 9*c*) and can reach branching fractions of $\mathcal{O}(10^{-5})$ (96).

With production rates of $O(10^3$–$10^4)$ per year (see Table 1), such events could be studied at the LHC only if they are given high priority in triggering during high-luminosity running, because suppressing large standard-model backgrounds will translate into small signal efficiencies. At a linear collider, production rates are at most $O(1$–$10)$ per year, but low background and very high (∼90%) signal efficiency may make these processes observable, should they occur.

3.2.2. SUPERSYMMETRIC DECAYS OF THE TOP QUARK In SUSY, the large Yukawa coupling of the top quark can lead to large mass splitting among the superpartners

[8]Low energy limits on FCNCs may be explained by tuning of the Yukawa matrices.
[9]These branching fractions can be enhanced by more than a factor of 10 under favorable conditions in the MSSM.

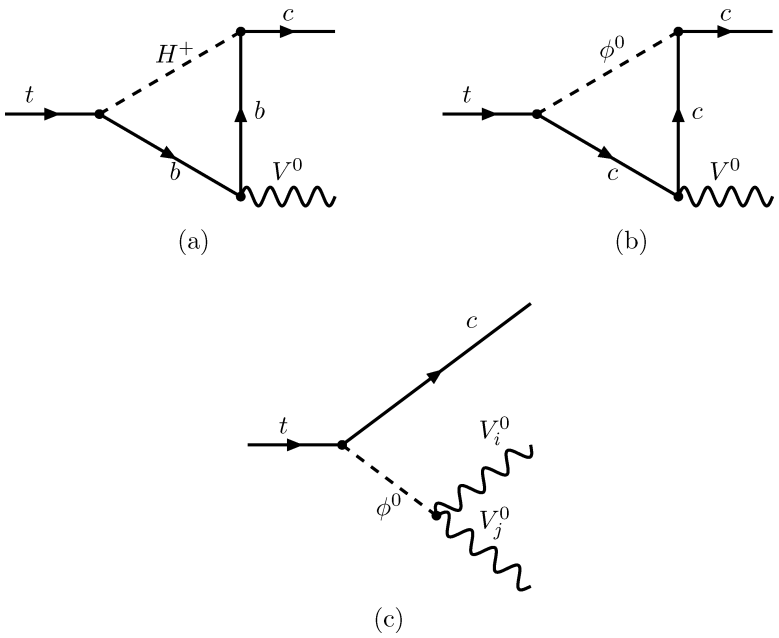

Figure 9 One-loop diagrams for $t \to cV^0$ (a, b) and tree diagrams for $t \to cV_i^0V_j^0$ (c) in 2HDM. $V^0 = \gamma, Z, g$; $\phi^0 = h^0, H^0, A^0$.

of the third-generation fermions. The superpartners of the right-handed and left-handed top quark combine to form mass eigenstates $\tilde{t}_1$ and $\tilde{t}_2$. The lightest top squark, $\tilde{t}_1$, can be lighter than all other squarks, and in fact can have mass near m_t. Naturally, this has implications for possible top-quark decays. We first address top SUSY decays under the assumption that $\mathcal{R}$ parity[10] is conserved. Afterward, we drop this assumption.

$\mathcal{R}$-parity conservation requires superparticles to be produced in pairs and forbids decays of the lightest supersymmetric particle (LSP). The LSP is widely assumed to be the lightest neutralino, $\tilde{\chi}_1^0$ (neutralinos are the sfermion partners of the standard-model bosons). Under this assumption, the most likely top SUSY decay is $t \to \tilde{t}_1\tilde{\chi}_1^0$. Generally, the top squark will decay via $\tilde{t}_1 \to c\tilde{\chi}_1^0$ or $b\tilde{\chi}_1^+$, depending on the various daughter masses. In the latter case, $\tilde{\chi}_1^+ \to \tilde{\chi}_1^0\ell\nu_\ell$ or $\tilde{\chi}_1^0 q_1\bar{q}_2$. The neutralinos interact only weakly, so they generally escape without detection, like neutrinos.

Branching fractions as large as 0.4–0.5 are possible for $t \to \tilde{t}_1\tilde{\chi}_1^0$ (97). In such a scenario, about half of $t\bar{t}$ events would have one standard-model and one

[10] $\mathcal{R}$ parity is a discrete, multiplicative symmetry imposed to inhibit baryon-number- and lepton-number-changing processes. It is defined as $\mathcal{R}_p \equiv (-1)^{3B+L+2S}$, where B is baryon number, L lepton number, and S spin.

SUSY top decay. The CDF experiment searched Run 1 data for events of this type, in which the standard-model top decay proceeds as $t \to Wb \to \ell\nu_\ell b$ ($\ell = e, \mu$) while the SUSY decay of the other top quark proceeds as $t \to \tilde{t}_1\tilde{\chi}_1^0 \to b\tilde{\chi}_1^+\tilde{\chi}_1^0 \to bq_1\bar{q}_2\tilde{\chi}_1^0\tilde{\chi}_1^0$. The signal consists of a lepton, $\not\!\!E_T$, and four jets (including the two b jets)—identical to standard-model single-lepton decay but differing in p_T and angular distributions. These depend on the masses of the particles involved. Under the assumptions $\mathcal{B}(\tilde{\chi}_1^\pm \to \ell\nu\tilde{\chi}_1^0) = \frac{1}{9}$, $\mathcal{B}(\tilde{t}_1 \to b\tilde{\chi}_1^\pm) = 1$, and $B(t \to \tilde{t}_1\tilde{\chi}_1^0) + B(t \to Wb) = 1$, the search excluded $B(t \to \tilde{t}_1\tilde{\chi}_1^0) > 0.45$ at 95% CL over most of the kinematically allowed $[m_{\tilde{t}_1}, m_{\tilde{\chi}_1^\pm}]$ parameter space for $m_{\tilde{\chi}_1^0}$ up to 40 GeV (98). For larger LSP masses, the kinematically allowed region shrinks.

The alternative scenario, $t \to \tilde{t}_1\tilde{\chi}_1^0 \to c\tilde{\chi}_1^0\tilde{\chi}_1^0$, is similar in character to the FCNC decay $t \to cZ \to c\nu\nu$. In the most promising channel, one top quark undergoes the non-standard-model decay while the other follows the standard model. If the W decays leptonically, then the signal consists of a high-p_T isolated lepton, substantial $\not\!\!E_T$, and two jets, one of which is a b. The large background from $W(\to \ell\nu) + \geq 2$ jets limits the search to regions of parameter space where $m_{\ell\not\!\!E_T} > M_W$. If, on the other hand, the W decays hadronically, then we have four high-p_T jets and large $\not\!\!E_T$ for the signal. Backgrounds arise chiefly from $W(\to \tau\nu) + \geq 3$-jets events in which the tau is misidentified as a jet, and from $Z(\to \nu\nu) + \geq 4$ jets. The effectiveness of b tagging is reduced because there is only one b jet per event. Sensitivity is further compromised in much of the $[m_{\tilde{t}_1}, m_{\tilde{\chi}_1^0}]$ parameter space where the jet and $\not\!\!E_T$ spectra are soft and/or broad. Tevatron Run 1 data were statistically insufficient for this analysis, but that will change in Run 2.

$\mathcal{R}$-parity-violating ($\not\!\!R_p$) interactions in the MSSM greatly enhance FCNCs (99). Within a single coupling scheme, either the up-type quarks or the down-type quarks can avoid these processes, but not both simultaneously. The consequences of $\not\!\!R_p$ have been studied via measurements of K^0–$\bar{K}^0$, D^0–$\bar{D}^0$, and B^0–$\bar{B}^0$ mixing, and of $B(K^+ \to \pi^+\nu\bar{\nu})$. These measurements have produced constraints on the $j = 1, 2$ elements of the $3 \times 3 \times 3/\not\!\!R_p$ coupling matrix λ'_{ijk} (i, j, k are generation indices), but they leave the third generation somewhat unconstrained. If sleptons lighter than the top quark exist, then $t_L \to d_{Rk}\tilde{\ell}_i^+$ followed by $\tilde{\ell}_i^+ \to \tilde{\chi}_0\ell_i$ and $\tilde{\chi}_0 \to \bar{\nu}_i\bar{b}d_k$ can lead to a fairly clean signature ($\not\!\!R_p$ implies that the $\tilde{\chi}_0$, assumed here to be the LSP, is not stable). Future searches for such signals will constrain λ'_{i3k} ($k \neq 3$).

3.2.3. TOP DECAYS IN TOPCOLOR-ASSISTED TECHNICOLOR In technicolor theories (100), electroweak symmetry is hidden by chiral symmetry breaking of technifermions that transform nontrivially under a new strong gauge interaction called technicolor (TC). This yields correct weak boson masses if the scale of TC interactions is about 1 TeV. Fermion masses arise without fundamental scalars through the action of an additional, spontaneously broken gauge interaction called extended technicolor (ETC) (101). However, ETC interactions cannot account for the large mass of the top quark (102).

Topcolor-assisted technicolor (TC2) is an attempt to address this deficiency (63). In the simplest version, the third (heavy, h) generation is assumed to transform with

16 Jul 2003 16:50 AR AR199-NS53-09.tex AR199-NS53-09.sgm LaTeX2e(2002/01/18) P1: IKH

the usual quantum numbers under strong $SU(3)_h \times U(1)_h$, whereas the lighter (ℓ) generations transform identically under a different (weaker) group, $SU(3)_l \times U(1)_l$. At scales of about 1 TeV, $SU(3)_h \times SU(3)_l$ and $U(1)_h \times U(1)_l$ spontaneously break down to ordinary color $SU(3)_C$ and weak hypercharge $U(1)_Y$, respectively. EWSB is still driven primarily by TC interactions, but topcolor interactions, felt only by the third-generation quarks (also at a scale near 1 TeV), generate the very large top-quark mass. ETC interactions would still be required to generate the light fermion masses and a small but important contribution to the mass of the top quark $m_t^{\rm ETC}$. The reason for a nonzero $m_t^{\rm ETC}$ is to give mass to the "top pions," the Goldstone bosons of (t, b) chiral symmetry breaking.

In TC2 models, the $tb\pi_T^+$ coupling is small, but the $tb\pi_t^+$ coupling is large, and the ETC interactions responsible for the small component of m_t induce mixing between top pions and technipions. The consequence is a possibly significant partial width (if kinematically allowed):

$$\Gamma(t \to \pi_t^+ b) = \frac{|\epsilon|^2}{16\pi} \left(\frac{m_t^{\rm dyn}}{m_t} \right)^2 \frac{\left(m_t^2 - m_{\pi_t}^2\right)^2}{F_t^2 m_t}, \qquad 5.$$

where ϵ is the top-pion component of the technipion mass eigenstate, $m_t^{\rm dyn}$ the dynamical top-quark mass, m_{π_t} the technipion mass, and F_t (≈ 70 GeV) the top-pion decay constant. Short of direct discovery, a precise experimental determination of Γ_t is required to limit the allowed parameter space in these models.

4. TOP-QUARK PROPERTIES

Confirmation of the standard-model nature of the top quark requires that we measure all its quantum properties and compare the measurements with standard-model expectations. Deviations would indicate new physics. In this section, we describe the status of these measurements, our future expectations, and the crucial experimental and theoretical issues.

4.1. Mass

The top quark is the least well-studied quark in terms of quantum properties, but its mass, m_t, is more precisely known (as a fraction of its mass) than that of any other quark. This is extremely important because the top quark plays a proportionally more important role in standard-model precision fits than any other quark. Top's importance is an artifact of EWSB and the large value of the top-quark Yukawa coupling, Y_t. The fact that Y_t appears to be exactly 1 has not gone unnoticed. Proponents of strong dynamical EWSB argue that the large top mass supports this class of theories because in general they predict large values of Y_t, on the order of 1 or more. On the other hand, the large top mass is also generally regarded as support for SUSY extensions to the standard model, which would not be

viable unless the top-quark mass were large; the running of $\sin^2\theta_W$ could not be made to fit the data and still allow for gauge-coupling unification otherwise, and EWSB would not occur, since the large value of the top-quark Yukawa coupling is what drives the coefficient of the Higgs-mass term negative. But large m_t does not clearly select either class of theories. One is left with the simple suspicion that the top quark is perhaps connected to new physics on the grounds that physical parameters of exactly 1 (or 0, etc.) indicate a more fundamental property underlying Y_t.

The impact of m_t elsewhere varies. In B and K physics, many observables have terms roughly quadratic in m_t/M_W. It was, in fact, data from B_0–$\bar{B}_0$ mixing in 1987 that first indicated a heavy top quark. For precision standard-model electroweak fits, m_t enters quadratically in many places as well. Examples are the $Z \to b\bar{b}$ decay rate R_b, the $e^+e^- \to f\bar{f}$ asymmetry A_{LR}, the weak mixing parameter $\sin^2\theta_W$, and the parameter $\rho \equiv \frac{M_W^2}{M_Z^2 \sin^2(\theta_W)}$. The corrections usually appear as a multiplicative factor, $1 + \frac{3G_F m_t^2}{8\sqrt{2}\pi^2}$. The W mass, which is not known nearly as precisely as most of the other quantities in the electroweak sector, receives quantum corrections proportional to m_t^2 and $\ln(M_H)$, where M_H is the Higgs-boson mass. The influence of m_t and M_H on M_W is usually plotted as m_t versus M_W, overlaid with bands that show the predicted M_H, as in Figure 1. A "light" Higgs is favored, somewhere around 100 GeV, but with an uncertainty of $O(100)$ GeV. The weak (logarithmic) dependence on M_H and the difficult-to-quantify sensitivity to new physics mean that one cannot draw firm conclusions from the fits. As the precision of m_t and M_W improves, however, and if a Higgs boson remains unobserved, the fit increasingly suggests breakdown of the standard model.

The current precision in m_t ($\delta m_t \sim 5$ GeV) achieved from Tevatron Run 1 is sufficient not only for the current precision of B and K physics experiments but even for the next generation of K experiments. Once the W-mass precision reaches 20 MeV, m_t must be known within 3 GeV in order not to limit the electroweak precision fit for M_H. Indeed, such a precision for m_t is a goal of the Tevatron Run 2. For a future linear collider, the 6-MeV precision on M_W must be matched by 1-GeV precision on m_t.

Both the LHC and a linear collider can outperform these goals. At the LHC, $\delta m_t \simeq 2$ GeV is expected within one year of low-luminosity running, and 1 GeV could be achieved with the $\ell J/\psi$ final state (discussed shortly) and a larger data set (20). Precision approaching 100 MeV can be obtained at a future linear collider with a $t\bar{t}$ threshold scan (103), which does not measure the pole mass and so is not limited by uncertainties of $O(\Lambda_{\rm QCD})$.

One specific case that would require a super-precise determination of m_t is the discovery of low-energy SUSY. In the MSSM, the mass of the lighter CP-even neutral Higgs boson h is given at the NLO by

$$M_h^2 \;=\; M_Z^2 \;+\; \frac{3G_F}{\pi^2\sqrt{2}}\, m_t^4 \ln\!\left(\frac{M_S^2}{m_t^2}\right), \qquad 6.$$

where M_S^2 is the average of the two top squark squared masses. Since a linear collider could measure M_h to about 50 MeV precision (103), m_t would need to be known to 100 MeV or better to permit incisive SUSY-electroweak precision fits. Ironically, this would require M_h to be known to probably the four-loop level; only two-loop calculations are currently available. One is forced to wonder whether the requisite improvement in theoretical precision could realistically be expected.

We now highlight the principles behind top-quark mass measurements made so far at the Tevatron. Details and subtleties can be found elsewhere (4–6, 8, 20, 104, 105). The main idea is to compare the observed kinematic features of $t\bar{t}$ pairs to those predicted for different top-quark masses. Although many kinematic variables are sensitive to m_t, explicit reconstruction from the $t\bar{t}$ decay products is an obvious choice, as long as we understand that it is uncertain at least to $O(\Lambda_{\rm QCD})$. However, more elaborate methods that attempt to connect many observables simultaneously with the matrix elements of the production and decay processes on an event-by-event basis are gradually emerging as a superior alternative.

There are three channels to consider, depending on how the two top quarks decay: dilepton, single-lepton, and all-hadronic. Here, "lepton" refers to electrons and muons only, since the presence of additional neutrinos in tau decays severely limits the usefulness of $t\bar{t} \rightarrow \tau X$ channels in the m_t determination. Thus, the branching fractions of the three channels are approximately 0.05, 0.30, and 0.44, respectively. Signal and background characteristics vary from channel to channel, so the exact technique used must be tailored accordingly for each channel.

For direct reconstruction of invariant masses of the two top quarks in a $t\bar{t}$ candidate event, one needs to know the four-momenta of the six daughters, a total of 24 quantities. Imagine an ideal $t\bar{t}X$ event with no final-state radiation in which the momentum of X, which represents everything recoiling against the $t\bar{t}$ system, is fully measured. If the three-momenta of n of the six final-state objects are directly measured, we have $3n$ measured quantities from the two top-quark decays. The masses of the six decay products are known (these can be safely assumed zero), as are the two intermediate W masses. Although m_t is yet unknown, it must be the same for both top quarks in the event. So we have nine constraints from particle masses.[11] That the $t\bar{t}X$ system carries no significant momentum transverse to the beamline gives two additional constraints:[12] $\vec{p}_T(t\bar{t}X) = 0$. Thus, a kinematic mass fit is subject to $(3n + 9 + 2 - 24) = (3n - 13)$ constraints. For each leptonic W decay, there is a corresponding neutrino that cannot be directly observed. Therefore, $n = 6$ for all-hadronic, $n = 5$ for single-lepton, and $n = 4$ for dilepton events. Dilepton events are underconstrained (-1C), preventing explicit reconstruction of the top mass from the daughters, so one must seek alternative means.

In every channel, many factors complicate m_t measurement. The observed objects' momenta need to be corrected to remove detector effects. The lion's share

[11]One must appropriately allow for Γ_W and Γ_t.

[12]In general, $x_1 \neq x_2 \Rightarrow p_z(t\bar{t}X) \neq 0$.

of the uncertainty in these corrections is due to jet-energy measurements. Any sampling calorimeter has a relatively large inherent uncertainty in its absolute energy scale. Moreover, the detector geometry has nonuniformities, such as module boundaries and ~~gaps or "cracks,"~~ to allow passage of cables and other hardware. Therefore, the response must be carefully mapped as a function of where the jet traversed the detector. Detector response is often a nonlinear function of jet energy. Additionally, each element of a calorimeter, or "cell," has a minimum threshold to register energy. Jet reconstruction proceeds by identifying clusters of (nearly) contiguous cells registering energy. These effects need to be understood and carefully accounted for. Two other effects arise from the nature of hadron-collider events. Each $t\bar{t}$ hard scattering gives rise to an associated underlying event from the proton/antiproton remnants, which deposits soft energy through the calorimeters. Also, in high-luminosity running, each $t\bar{t}$ event is embedded in multiple interactions, dominated by soft-inelastic $p\bar{p}$ or pp scattering, that contaminate the energy measurement.

Other complications are more related to the physics of the $t\bar{t}$ event itself. One is that we often find jets that do not even originate from top-quark decays directly but rather from initial- or final-state radiation (106). Owing to detector segmentation or limitations in the reconstruction algorithms, two or more jets can be merged and reconstructed as one. Sometimes the opposite occurs: Fragmentation causes a single jet to split in two. Occasionally, a jet is lost entirely because it travels through an uninstrumented or poorly instrumented region, such as the beam pipe. These extra or missing jets result in the entry of extraneous solutions into reconstructed m_t distributions.

Because the all-hadronic channel has a large branching fraction and is maximally constrained, one might surmise that it would be the best for measuring m_t. In practice, however, a very large and hard-to-model QCD multijet background, compounded by the jet-measurement issues mentioned above, leads to relatively large uncertainties. The top-quark mass extracted by CDF (107) in the all-hadronic channel is $186.0 \pm 10(\text{stat.}) \pm 5.7(\text{syst.})$ GeV. Each event is required to have six or more jets and to satisfy several topological requirements that help improve the S:B ratio. Events were reconstructed to the $t\bar{t} \to W^+bW^-\bar{b} \to q_1\bar{q}_2bq_3\bar{q}_4\bar{b}$ hypothesis using the six highest-E_T jets, one of which must be b-tagged. This still leaves 30 different reconstruction combinations. A kinematic fit constrains each combination to yield M_W for two jet pairs, equal t and $\bar{t}$ masses, returning a χ^2 value. The combination with the smallest χ^2 is chosen. The resulting "reconstructed-mass" distribution from the candidate events is then compared, through a likelihood fit, to templates formed from the right mix of $t\bar{t}$ (from simulation) and QCD background, the shape of which is extracted from data. The input m_t is changed and the value that maximizes the likelihood L is the central value of the top-quark mass measurement. The statistical uncertainty is determined from the range over which the $-\ln L$ increases by $\frac{1}{2}$ unit with respect to its minimum. An analysis of the all-hadronic final state by DØ, which is similar in spirit but employs a neural-network algorithm to compensate for a lower b-tagging efficiency, is approaching completion. ~~The preliminary result is $176^{+17.1}_{-13.6}$ GeV.~~

16 Jul 2003 16:50 AR AR199-NS53-09.tex AR199-NS53-09.sgm LaTeX2e(2002/01/18) P1: IKH

The ultimate precision achievable in this channel is not expected to rival that of the single-lepton or dilepton channels but can still be used in a combined result to help reduce the overall uncertainty. A top-quark mass measurement in this channel is important on its own merits because it confirms that the excess of tagged six-jet events indeed comes from the top quark, or at least from a particle with a mass consistent with that measured in the other decay modes. Analysis of this final state is not very likely to be feasible at the LHC.

To permit a kinematical fit to the top-quark mass by a method similar to the one discussed above, in addition to an isolated high-p_T electron or muon in the central region of the detector, a single-lepton candidate event is required to have at least four jets. This sample is much cleaner than the all-hadronic channel but still suffers from combinatorial ambiguities in the reconstruction. Including the two-fold ambiguity in the neutrino p_z, the ambiguity is fourfold if both b jets are tagged, 12-fold if only one b is tagged, and 24-fold without b tagging. Run 1 results in this channel are 173.3 ± 5.6(stat.)± 5.5(syst.) GeV [DØ (4)] and 176.1 ± 5.1(stat.) $\pm$ 5.3(syst.) GeV [CDF (8)].

It is interesting to note that even when both b jets are tagged, Monte Carlo simulations suggest that in only about half of the cases does the best χ^2 correspond to the correct matching of the four leading jets to the appropriate quarks. The other half are roughly equally split between instances in which all jets are matched to partons, but the lowest χ^2 did not choose the combination with the correct assignments, and instances in which there are extra jets from initial- or final-state radiation and the four leading partons from the $t\bar{t}$ decay cannot be uniquely matched to the four leading jets in the event. At the LHC, ~~$t\bar{t}$ events~~ χ^2 will have higher p_T, on average. This will often mean that the daughters of the two top quarks will be on opposite sides of a plane. Such hemispheric separation will considerably alleviate these combinatorial problems.

A more recent analysis in the single-lepton channel by DØ (5) makes a comparison of data with LO matrix elements on an event-by-event basis, similar to that used for the dilepton channel discussed below (84, 108). This analysis requires the number of jets in a candidate event to be exactly four and accords no special status to events with b-tagged jets. A likelihood function is formed taking into account all possible permutations of jet assignments, not just that with the lowest χ^2. The main difference between this method and the previous one is that each event now has an individual probability as a function of m_t. This probability, reflecting both signal and background, depends on all measured variables in the event (except unclustered energy), with well-measured events carrying more weight in the extraction of m_t than poorly measured events. The preliminary result, $m_t = 179.9 \pm 3.6$(stat.) $\pm$ 6.0(syst.) GeV, reflects a marked reduction of the statistical uncertainty relative to the previous result, which was based on the same data but relied heavily on explicit reconstruction of invariant masses.

Two alternatives to invariant-mass reconstruction have been tried to measure m_t in the kinematically underconstrained dilepton channel, $t\bar{t} \rightarrow \ell_1\nu_1 b\ell_2\nu_2\bar{b}$, which also suffers from the smallest branching fraction. In the first (108), one

16 Jul 2003 16:50 AR AR199-NS53-09.tex AR199-NS53-09.sgm LaTeX2e(2002/01/18) P1: IKH

hypothesizes a mass for the top quark, reconstructs the neutrino momenta with a fourfold ambiguity for each lepton–b pairing, and calculates the probability that the final-state configuration will come from a $t\bar{t}$ event of that m_t. For each event, a set of assumed masses produces probability distributions to use as event weights. The preferred m_t for an event can be taken as the maximum or the mean of the distribution. The distribution of preferred masses for a set of candidate events is compared through a likelihood method to the expected distribution from a combination of signal and background for a given m_t. As in the other channels, the central value of the measurement is the value with maximum likelihood.

Variants of this technique make use of more or fewer assumptions about $t\bar{t}$ production details to obtain the event probabilities. For example, DØ reported two different measurements, one that used neutrino kinematic distribution weights and another that used production and decay terms in the matrix element for the weights. The methods yielded very consistent results. The final result is (6, 104) $m_t = 168.4 \pm 12.3(\text{stat.}) \pm 3.6(\text{syst.})$ GeV.

CDF's measurement in the dilepton channel used only information about the expected pseudorapidity distributions of the neutrinos. These were chosen randomly from Monte Carlo predictions; then the two neutrino momenta were solved for. Each solution (ambiguity included) was assigned a weight according to how well the derived and measured $\vec{\not{E}}_T$ matched. CDF's result is (8, 104) $m_t = 167.4 \pm 10.3(\text{stat.}) \pm 4.8(\text{syst.})$ GeV. CDF also used a likelihood fit to kinematical variables that are sensitive to m_t: the b-jet energy spectrum and the full event-invariant mass (109). Results from these are consistent but suffer larger systematic uncertainties.

The other method for the dilepton channel (84) is based on the observation that, modulo finite-W-width effects, the b-quark energy is fixed in the top-quark rest frame. The top-quark mass is then given by $m_t^2 = \langle m_{b\ell}^2 \rangle + \sqrt{M_W^4 + 4M_W^2 \langle m_{b\ell}^2 \rangle + \langle m_{b\ell}^2 \rangle^2}$, where $\langle m_{b\ell}^2 \rangle$ is the mean value of $m_{b\ell}^2$ in the sample. The results are generally consistent with those of the likelihood methods.

The dilepton sample also contains a subsample of events that may help reduce uncertainties at the LHC. In this subsample, one looks for events in which one of the b quarks hadronizes to J/ψ, which subsequently decays to $\ell^+\ell^-$, providing a cleaner and more precisely measured sample. When the sister W decays leptonically to $\ell' \nu_{\ell'}$, a strong correlation exists between m_t and $m_{J/\psi\,\ell'}$ (110). The top-quark mass can be extracted essentially from the endpoint of the Gaussian $m_{J/\psi\,\ell'}$ distribution. In recent improvements to HERWIG, matrix-element corrections to radiative top-quark decays are known to cause a 1–1.5-GeV shift in the extracted m_t (111). Ongoing study of this endpoint spectrum must take into account this Monte Carlo improvement in order to attain the goal of 1-GeV precision in this channel.

The Tevatron average for m_t is $174.3 \pm 3.2(\text{stat.}) \pm 4.0(\text{syst.})$ GeV (7). Figure 10 shows the breakdown per channel and the global average. Table 3 summarizes the systematic uncertainties in the DØ and CDF Run 1 m_t measurements

TABLE 3 Channel-by-channel systematic uncertainties (GeV) in Tevatron Run 1 top-quark mass measurements

Channel →	**Dilepton**		**Single-lepton**		**All-hadronic**	
Systematic uncertainty	**CDF**	**DØ**	**CDF**	**DØ**	**CDF**	**DØ**
Jet-energy scale	3.8	2.4	4.4	4.0	5.0	?
Model for signal	2.8	1.7	2.6	1.9	1.8	?
Monte Carlo generator	0.6	0.0	0.1	0.0	0.8	?
Uranium noise/multiple interactions	0.0	1.3	0.0	1.3	0.0	?
Model for background	0.3	1.0	1.3	2.5	1.7	?
Method for mass fitting	0.7	1.1	0.0	1.5	0.6	?
Total	4.8	3.6	5.3	5.5	5.7	?

insert a horizontal line

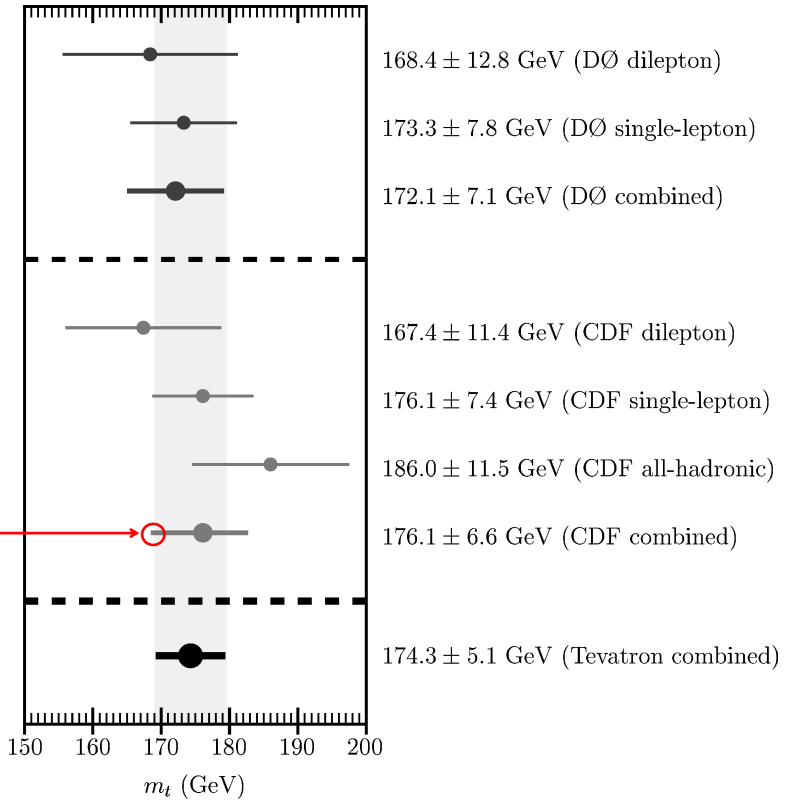

1 GeV too low. Fixed figure mailed to Kim.

Figure 10 Tevatron measurements of top mass in different final states, and the combined result.

in the various channels. As mentioned above, most of the systematic uncertainty comes from the jet-energy scale. Experimenters need to understand and maintain the calibration of their calorimeters to high precision to help keep part of this systematic uncertainty under control.

With larger samples of events in Run 2 and at the LHC, both statistical and systematic uncertainties will be reduced significantly. There are several reasons for this. First, one can afford to narrow the focus to samples with two b-tagged jets. This reduces combinatorics but also reduces energy-scale uncertainty, since energy corrections specific to b jets can be applied to help with the mass resolution. One can also choose specific subsets of events in which, for example, the exact number of jets as expected from the top quark are found and the jet energies are particularly well-measured (whether fiducially or owing to high energy). Events with particular topologies can similarly help. ATLAS and CMS plan to use angular information and possible hemispheric separation of the two top quarks as well, to assist in assigning the correct b–W combination. Additionally, with large-integrated-luminosity samples, the control samples used to map the calorimeters' energy responses, such as photon + jets and high-E_T dijets, will be less statistically limited and will help reduce the jet-energy-scale uncertainty.

Another source of improvement in the mass measurement can come from a better understanding of the treatment of initial- and final-state radiation. If the parton came from initial-state radiation, including it in the reconstruction would bias m_t toward larger masses. If it instead came from radiative top-quark decay or from the final-state b quark, it must be included, lest the inferred value of m_t be too low. This issue has been known for a long time and has been addressed at the theoretical level with exact calculations of the expected rates and radiation patterns for one additional hard parton (36). Orr and collaborators propose to assign additional hard jets in events to either production or decay by calculating the following observables:

$$S_{\text{prod}} = \left|\left[(p_{W^+} + p_b)^2 - m_t^2 + im_t\Gamma_t\right]\left[(p_{W^-} + p_{\bar{b}})^2 - m_t^2 + im_t\Gamma_t\right]\right| \quad 7.$$

$$S_1 = \left|\left[(p_{W^+} + p_b)^2 - m_t^2 + im_t\Gamma_t\right]\left[(p_{W^-} + p_{\bar{b}} + p_j)^2 - m_t^2 + im_t\Gamma_t\right]\right| \quad 8.$$

$$S_2 = \left|\left[(p_{W^+} + p_b + p_j)^2 - m_t^2 + im_t\Gamma_t\right]\left[(p_{W^-} + p_{\bar{b}})^2 - m_t^2 + im_t\Gamma_t\right]\right|. \quad 9.$$

The extra jet is assigned to "production" if $S_{\text{prod}} < \min(S_1, S_2)$ and "decay" otherwise. This assumes, of course, that in samples containing hadronic W decays, the correct assignment has already been made for the W jets (i.e., a radiative W decay could be identified). How well the idea may apply under experimental constraints remains to be evaluated.

4.2. Spin

All standard-model fermions have a left-handed weak gauge coupling, which mediates their decays, if they decay. Only the top quark, because it is so massive, decays before it hadronizes or its spin flips, thus leaving an imprint of its spin at

16 Jul 2003 16:50 AR AR199-NS53-09.tex AR199-NS53-09.sgm LaTeX2e(2002/01/18) P1: IKH

production on its angular decay distributions. But how do we even know that the top-quark candidate is a fermion? First, if it were spin 0 or 1, we would have to postulate an additional unobserved daughter to conserve overall spin. Furthermore, although the Tevatron and the LHC use unpolarized beams and therefore produce unpolarized top-quark pairs, for spin 0 their spins would not be correlated, whereas for spin 1 they would be, although this correlation has not been considered. The spin correlations arising from a spin 3/2 scenario have also not been considered. However, a simple argument against spin 3/2 is that the $t\bar{t}$ cross section would be much larger. This was in fact how the tau lepton was determined to be spin 1/2.

As a spin-1/2 fermion, the standard-model top quark has decay angular distributions $d\Gamma/d(\cos\theta_i^*) \propto 1 + \alpha_i \cos\theta_i^*$, where θ_i^* is the angle of decay particle i in the top-quark rest frame with respect to the top-quark spin ($i = \ell^+, \nu, b$, or $\bar{d}, u, b$), and α_i is the "spin analyzing power" of particle i. At leading order, $\alpha_i = 1, -0.32, -0.41$ (α_i have opposite signs for top quark and antitop quark), making the outgoing charged lepton or down-type quark that is not tagged as a b the ideal spin-correlation analyzer. If one uses the down-type quark in hadronic W decays, the QCD NLO corrected value must be used (112): $\alpha_{\bar{d}} \simeq 0.93$. For top-quark pair production, because the spins are correlated, one plots a double differential distribution (113, 114),

$$\frac{1}{\sigma}\frac{d^2\sigma}{d(\cos\theta_i)d(\cos\theta_{\bar{i}})} = \frac{1}{4}(1 - C\,\alpha_i\,\alpha_{\bar{i}}\cos\theta_i\cos\theta_{\bar{i}}), \qquad 10.$$

where $\theta_i(\theta_{\bar{i}})$ is now the angle of the ith($\bar{i}$th) decay product with respect to the chosen spin axis in the top (antitop) quark rest frame; and C is the spin-correlation coefficient—the relative fraction of like-spin top quarks produced in the spin basis considered. Near threshold, $t\bar{t}$ produced by quark pairs is in a $^3S_1$ state, whereas gluon production yields a $^1S_0$ state, so the two components will have different spin correlations, $C_{q\bar{q}}$ and C_{gg}. Observing the overall correlation would confirm that the top quark is indeed the standard-model partner of the bottom quark with a left-handed weak coupling.

The overall spin correlation coefficient C varies strongly depending on spin basis and which initial-state parton type dominates. Because $t\bar{t}$ production at the Tevatron is predominately quark-initiated, whereas at the LHC it arises mostly from initial gluons, different spin bases optimize analyses for the two machines. At the Tevatron, this is the "off-diagonal" basis of Reference (114), where the spin-basis angle ψ with respect to the proton beam direction is a function of the speed and production angle θ_t of the top quark with respect to the incoming p direction in the zero-momentum frame:

$$\tan\psi = \frac{\beta^2 \sin\theta_t \cos\theta_t}{1 - \beta^2 \sin^2\theta_t}. \qquad 11.$$

This basis is illustrated in Figure 11 (114). At the LHC, the "helicity basis" is optimal, which resolves spin along the flight direction of the top quarks in the zero-momentum frame. The NLO corrections to C are known to be $O(10\%)$ and

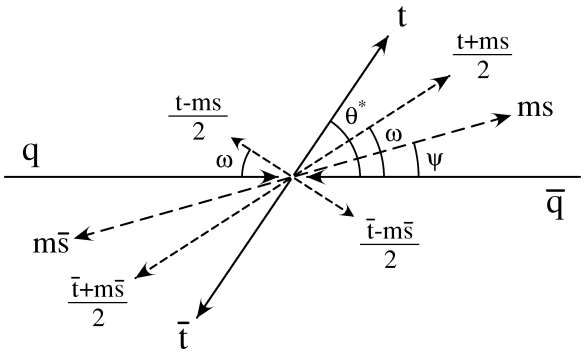

Figure 11 $t\bar{t}$ rest frame ("zero-momentum frame") for $q\bar{q} \to t\bar{t}$ at hadron colliders, from Reference (114). $t(\bar{t})$ are the (anti-)top quark momenta, $s(\bar{s})$ are the (anti-)top quark spin vectors. θ^* is the flight direction of the top quark, ψ is the direction of the off-diagonal spin bases, and ω is the preferred emission direction of the down-type fermion in top quark decay for up-down $(t + ms)$ and down-up $(t - ms)$ spin configurations. All angles are measured with respect to the p beam direction.

so will not greatly affect an analysis (115). However, the uncertainty in C even at NLO is unexpectedly large at the Tevatron. Because C_{gg} contributes with opposite sign to $C_{q\bar{q}}$, the overall value is quite sensitive to uncertainties in the gluon structure function at high x. Thorough study of PDF uncertainties will be required to resolve this. It is not as serious an issue at the LHC, as this process probes $g(x)$ at low x, where the PDF uncertainties are quite small, and in any case the scale uncertainty at NLO dominates over PDF uncertainties for this machine. At the Tevatron in the off-diagonal basis, $C_{\rm NLO} = 0.806^{+2.9\%}_{-4.0\%}(\mu)^{+4.0\%}_{-8.9\%}$(PDF), and in the helicity basis at the LHC, $C_{\rm NLO} = 0.311^{+6.4\%}_{-10.6\%}(\mu)^{+6.8\%}_{-0.0\%}$(PDF) (115).

Because the spin analyzing power of the charged lepton (leptonic decay) or d quark (hadronic decay) is maximal, they are the natural choice for observing the correlations. The dilepton $t\bar{t}$ sample has the least background contamination, but because of the two missing neutrinos can be reconstructed only statistically. Flavor tagging is not possible among the light quarks, but the down-type quark is typically the least-energetic quark in W decay in the top quark rest frame. In principle, then, use of the single-lepton and all-hadronic channels is possible, but needs further investigation.

If the top quarks decay isotropically, then $C = 0$ (no correlation). New physics such as CP violation or a right-handed tbW coupling would also alter the predicted value of C (116). The task then is to determine the achievable level of uncertainty on C at Tevatron and LHC. DØ has performed an analysis of their dilepton samples (10). While the statistics were too poor to give a strong result, they clearly established that the measurement can be performed. Run 2 expectations are that $C = 0$ can be ruled out at better than the 2σ level with 2 fb^{-1} of data. At the LHC, CMSJET simulation (20) estimates a measurement of $C = 0.331 \pm 0.023$

(statistical errors only, LO simulation) for the standard model, more than good enough to rule out the isotropic decay case. Polarimetry of the b quark has been proposed to enhance spin correlation analyses (117), but has not yet been investigated by the experimenters. Of course, the ultra-low-background environment, beam polarization, and $\sqrt{s}$ tuning of a linear collider would be ideal for precision spin and spin correlation measurements (118).

Because all three modes of single-top-quark production (Fig. 6) can be observed at both Tevatron and LHC, it is useful to consider spin for these cases as well. Here the interesting distribution is the angle θ between the charged lepton in the top quark decay and the chosen spin axis (119, 120):

$$\frac{1}{\sigma_T}\frac{d\sigma}{d\cos\theta} = \frac{1}{2}[1 + C'\cos\theta], \quad C' = \frac{N_\uparrow - N_\downarrow}{N_\uparrow + N_\downarrow}. \qquad 12.$$

where $N_{\uparrow(\downarrow)}$ is the number of top quark events produced spin up (down) in the frame considered. The spin asymmetry C' in this case is maximized by choosing the spin basis that most strongly correlates with the down-type quark on the production side. For W^* production, this is simply the antiproton direction at the Tevatron (119). The Wg-fusion process is more challenging due to NLO complications in the initial and final states as the zero-momentum frame cannot be defined. Here one optimally chooses the "η-beamline" basis, which is defined as the beamline most closely aligned with the forward-scattered quark that supplied the fusing W (119). For Wt production, the ideal basis is defined by the down-type fermion from both W decays (120). This channel has severe experimental problems reconstructing the top-quark rest frame for most decay channels but is under investigation.

One study (113) noted observation of the spin correlation is also a crucial test of the CKM matrix element V_{tb}. Because Γ_t is nearly proportional to $|V_{tb}|^2$ (assuming $|V_{tq}| \ll |V_{tb}|$ for $q = d, s$), if V_{tb} were small due to a fourth generation, then the top quark would decay on average after the spin-flip time $m_t/\Lambda^2_{\rm QCD}$—the spin correlation would not be seen! This provides the constraint $|V_{tb}| > 0.03$.

4.3. Charge

The electric charge of the top quark has not actually been measured. Although its value is widely supposed to be $Q_t = +2/3$, as predicted by the standard model, in some exotic theories the top quark is much heavier, and the Run 1 observation is of another exotic quark of charge $Q = -4/3$ (121). Techniques to measure the top charge directly at hadron colliders have been explored using the sample of single-lepton events that contain a hard photon (122): $t\bar{t} \to \gamma\ell\nu bjj\bar{b}$ (j is a jet from $W \to q_1\bar{q}_2$).

The photon can be radiated from any electrically charged particle in the process, which means that contributions arise from radiation in top-quark production (including quark initial states), radiative top-quark decay, and radiative W decay. The contribution of radiative W decay is standard-model-like, and its influence can be removed by requiring that the invariant mass of the $jj\gamma$ system and the

16 Jul 2003 16:50 AR AR199-NS53-09.tex AR199-NS53-09.sgm LaTeX2e(2002/01/18) P1: IKH

transverse mass of the $\ell\gamma\vec{\not p}_T$ system be larger than 90 GeV. Events are dominated by photons produced in top-quark production if one imposes the following cuts:

$$m(b_{1,2}jj\gamma) > 190 \text{ GeV}, \quad m_T(b_{2,1}\ell\gamma\vec{\not p}_T) > 190 \text{ GeV}. \qquad 13.$$

At Tevatron energies, photon radiation from the initial-state quark pairs (which contribute about 90% of $t\bar{t}$ events) dominates the cross section, so $Q_t = -4/3$ increases the cross section of this sample by only about 20%. At the LHC, however, where $gg \to t\bar{t}$ dominates, the cross section is enhanced by a factor of 2.6, since the cross section is roughly proportional to Q_t^2. Radiative-decay samples are chosen by selectively changing one of the relative symbols for the cuts of Equation 13. In these cases, the sample cross sections actually decrease if $Q_t = -4/3$, due to interference between radiation from the t, W, and b lines.

It is more useful to examine the p_T and angular distributions of photons for the three $t\bar{t}\gamma$ samples; these distributions are anomalous in the case of the exotic charge assignment. For example, the photon is typically closer to the lower-energy b quark. The distributions can be used to perform a χ^2 test to distinguish the $Q_t = +2/3, -4/3$ hypotheses. Q_t for this purpose is treated in the literature as a continuous rather than discrete quantity because the strict requirement of a viable electroweak model is simply that the two partners of an SU(2) doublet differ by one unit of charge. However, the models that allow for this realization are quite strange, so we choose to keep the two discrete charge assignments separate. Estimates are that Tevatron Run 2 would require some 20 fb^{-1} to confirm $Q_t = +2/3$ at 95% CL using the photon distributions, and the LHC would require 10 fb^{-1} to confirm $Q_t = +2/3$ at 100% CL. A 500-GeV linear collider could achieve this as well with $O(100)$ fb^{-1} of data (123).

Alternatively, one can look for a few very clean single-lepton $t\bar{t}$ events where either the b-jet charge is measured or the b from the leptonic top-quark decay decays semileptonically (122). Because $Q_t = Q_b + Q_\ell$, the latter could work even at the Tevatron if experiments are lucky enough to see a few such clean events. However, measuring b-jet charge is less well explored.

4.4. Gauge Couplings

We know from observing $p\bar{p} \to t\bar{t} \to b\bar{b}W^+W^-$ at the expected standard-model rate, and from the nonobservation of other decays (including radiative QED), that the top-quark gauge couplings to g, $W^\pm$, Z, and γ are roughly standard-model-like. These gauge couplings must now be measured precisely; anomalous coupling analyses are the most appropriate. *CP* violation in the top-quark sector is normally addressed in this language, via the *CP*-even and -odd terms in the effective Langrangians used.

The motivation for studying anomalous QCD top-quark gauge couplings is that they naturally arise in dynamical electroweak-symmetry-breaking models such as technicolor or topcolor. They have been explored for the Tevatron (71, 124, 125) and LHC ((20, 125) and references therein). The effective Lagrangian appears as

16 Jul 2003 16:50 AR AR199-NS53-09.tex AR199-NS53-09.sgm LaTeX2e(2002/01/18) P1: IKH

the standard-model term plus chromoelectric and chromomagnetic dipole moment terms,

$$\mathcal{L}_{t\bar{t}g} = \bar{t}\left[-g_s\gamma^\mu G_\mu - i\frac{g_s\hat{d}'_t}{2m_t}\sigma^{\mu\nu}\gamma_5 G_{\mu\nu} - \frac{g_s\hat{\mu}'_t}{2m_t}\sigma^{\mu\nu}G_{\mu\nu}\right]t. \qquad 14.$$

Both anomalous terms flip chirality; the chromomagnetic moment $\hat{\mu}'_t$ is *CP*-even and the chromoelectric moment $\hat{d}'_t$ is *CP*-odd, so that *CP*-even and -odd observables can separate their effects. Because the *CP*-even chromomagnetic moment interferes with the standard-model vertex, observables are potentially sensitive to the sign of the coupling. One calculational detail is that, for $gg \to t\bar{t}$ subprocesses, an additional dimension-five operator must be introduced to preserve gauge invariance; this corresponds to an effective $ggt\bar{t}$ four-point interaction. There is also a standard-model loop contribution to the chromomagnetic moment that depends on the Higgs-boson mass. For example, for $M_H = 100$ GeV, the standard-model loop leads to a 2.5% correction to $\sigma_{t\bar{t}}$ at the LHC, which is smaller than the expected measurement uncertainty (125). The same study shows that O(10–20)% changes can occur in models containing two Higgs doublets or additional matter content, such as the MSSM.

Unfortunately, Tevatron studies have shown that these moments lead mostly to overall $t\bar{t}$ rate changes because of threshold effects dominating the angular distributions. Only for very large values of d'_t, μ'_t might one expect to observe shape changes in such distributions as the top-quark emission angle in the center-of-mass frame, or for dileptonic decays at the Tevatron,

$$\widehat{O}_L = \frac{1}{m_t^3|P|^2}P\cdot(Q_+\times Q_-)\,P\cdot(Q_+ - Q_-), \qquad 15.$$

where P, Q_+, Q_- is the momentum vector of the proton, ℓ^+, ℓ^-, in the center-of-mass frame. Even then, the statistics at Run 2 may not be sufficient to explore this with confidence. Furthermore, constraints from $b \to s\gamma$ on the chromomagnetic moment are already an order of magnitude better than the Tevatron can achieve (125). The prospect for explicit *CP*-odd observables for the chromoelectric moment is greater, but further study with detector simulation and up-to-date Run 2 expectations is needed. Unfortunately, the literature on $t\bar{t}g$ anomalous couplings contains a wide variety of conventions, especially among LHC studies. The results of LHC studies are extremely difficult to compare, both with each other and with other experimental constraints, such as those from $b \to s\gamma$. This should be rectified in the near future, to clarify what exactly can be learned.

At hadron colliders, anomalous $t\bar{t}\gamma$ and $t\bar{t}Z$ couplings can be explored only via associated production, as electroweak s-channel contributions to top-quark pairs are far too suppressed relative to QCD. Up-to-date predictions for these standard-model rates may be found elsewhere (122, 126). No anomalous coupling analysis has yet been performed for these cases, beyond the top-quark charge measurement of $t\bar{t}\gamma$. At a linear collider, ~~the~~ $t\bar{t}\gamma$ and ~~$t\bar{t}$~~ can be studied quite precisely in direct $t\bar{t}$ production (103, 123).

Anomalous $t\bar{b}W$ couplings have been explored at hadron colliders in the context of $t\bar{t}$ production and decay (116) and, more recently, single-top production (20, 71, 72). For $t\bar{t}$ production, the previously discussed limit on right-handed W bosons in top-quark decay is part of this subject, but it is not normally discussed in anomalous coupling language. The effective Lagrangian is

$$\mathcal{L} = \frac{g V_{tb}}{\sqrt{2}} \left[W_\mu^- \, \bar{b} \, \gamma_\mu P_- \, t \; - \; \frac{1}{2M_W} W_{\mu\nu}^- \, \bar{b} \, \sigma^{\mu\nu} \left(F_2^L P_- + F_2^R P_+ \right) t \right] + \text{h.c.}, \quad 16.$$

where $W_{\mu\nu}^{\pm}$ is the field-strength tensor and $P_\pm = (1 \pm \gamma_5)/2$; $F_2^{L,R} = 0$ in the standard model. The non-standard-model term is proportional to the particle momentum, and is realized by an anomalous contribution to the cross section at high p_T. In practice, one uses the W, b, or bb systems, depending on which single-top-production component is isolated. Even with 2 fb^{-1} at the Tevatron, limits of approximately $-0.18 < F_2^L < +0.55$ and $-0.24 < F_2^R < +0.25$ could be achieved, assuming a 10% systematic uncertainty. At the LHC, the constraint would improve by a factor of 2–3. It is important that this theoretical study be followed up by a detector simulation to include systematic uncertainties, which will probably be limiting. The sensitivity of a linear collider would be better by up to an order of magnitude. As a final note, Reference (127) pointed out that CLEO data on $b \to s\gamma$ are already more constraining on right-handed tbW couplings than would be achievable at any planned future colliders.

4.5. Lifetime and V_{tb}

The CKM matrix element V_{tb} is intimately related to the top-quark lifetime, so it is natural to discuss them together, even though they are often treated as separate topics. We usually speak of the lifetimes of quarks (charm and bottom) and leptons (muon and tau), rather than their intrinsic widths, because they are some fraction of a second that is measurable in the laboratory. Indeed, it is such "long" lifetimes that allow high-resolution vertex detectors to see the displaced decay vertices of tau leptons and b and c quarks in collider experiments. Like the other fermions, the top quark decays only weakly. So does it also have a long life? Fortunately, no. The top quark lives about 4×10^{-25} s, almost an order of magnitude more fleeting than the time it takes for a colored particle to hadronize.

A particle's lifetime is the inverse of its decay width, $\tau = \hbar/\Gamma$. In fact, we calculated the top-quark lifetime by first calculating its decay width. For extremely short-lived states, it is more useful to discuss the width, rather than the lifetime. Neglecting the b-quark mass, at leading order the top-quark bW partial width is

$$\Gamma(t \to Wb) \; = \; \frac{G_F}{8\pi\sqrt{2}} \, m_t^3 \, |V_{tb}|^2 \left(1 \; - \; 3 \, \frac{M_W^4}{m_t^4} \; + \; 2 \, \frac{M_W^6}{m_t^6} \right) \; = \; 1.56 \, \text{GeV}. \quad 17.$$

The NLO result is 1.42 GeV (128). Note that the NLO value cannot be used in a LO matrix element calculation—it will give the wrong $B(t \to bW)$, because

the other couplings are at leading order! This partial width is proportional to $|V_{tb}|^2$, just as the other standard-model decays, $t \to sW, dW$, are proportional to $|V_{ts}|^2$, $|V_{td}|^2$, respectively. These are a $\approx 0.2\%$ correction to the total width, $\Gamma_t = \sum_q \Gamma(t \to Wq)$, if there are indeed only three generations of quarks, in which case $0.9990 < |V_{tb}| < 0.9993$. We can be confident that $|V_{tb}| \gg |V_{ts}|, |V_{td}|$ even without the low-energy unitarity constraints, from the CDF measurement (129)

$$\frac{B(t \to bW)}{B(t \to qW)} = \frac{|V_{tb}|^2}{|V_{tb}|^2 + |V_{ts}|^2 + |V_{td}|^2} = 0.94^{+0.31}_{-0.24}, \qquad 18.$$

which looks for the fraction of tagged b jets in $t\bar{t}$ decays.

It is interesting to consider what happens if there are more than three generations, in which case unitarity constraints on V_{tb} from low-energy data are virtually meaningless. From electroweak precision data, we know the ρ parameter quite precisely. For four generations, its value is (130)

$$\rho \simeq 1 + \frac{3G_F}{8\sqrt{2}\pi^2}\left[m_t^2|V_{tb}|^2 + m_{t'}^2|V_{t'b}|^2\right] = 1 + \frac{3G_F}{8\sqrt{2}\pi^2}\left[m_t^2 + \epsilon^2\left(m_{t'}^2 - m_t^2\right)\right], \qquad 19.$$

where t' is the up-type fourth-generation quark, and unitarity in the fourth generation requires that $|V_{tb}|^2 = 1 - \epsilon^2$, $|V_{t'b}|^2 = \epsilon^2$ (given our belief in very small V_{ts}, V_{td}). It is obvious that either ϵ is small or the top quark and the fourth generation up-type quark are nearly degenerate. The latter case would be discovered quite soon; the fourth-generation issue is not of great concern.

For unstable particles, the width exhibits itself as a spread in the invariant-mass distribution of the decay products, the Breit-Wigner lineshape. Unfortunately, the top-quark width is narrower than experimental resolution at a hadron collider, so neither the Tevatron nor the LHC will be able to determine it directly. (One can set limits comparable to the detector resolution, but these will never be competitive with branching-faction checks and other methods.) However, it will be possible to determine the top-quark width indirectly, by combining several results that depend on Γ_t. To do so requires observation of both $t\bar{t}$ and single-top production (in at least one of the three channels) and some mild theoretical assumptions that can be checked, within limits, via detailed studies of decay angular distributions. One must assume that QCD governs the $t\bar{t}$ production and that the $t\bar{b}W$ vertex is the standard $SU(2)_L$ weak gauge vertex; both assumptions are eminently reasonable and can be checked via anomalous couplings analyses discussed above, that look for deviations in various differential distributions and so do not rely solely on the total rate. All the necessary cross sections are known at NLO or better.

The measurement is linked to $|V_{tb}|$. First, one measures $\sigma_{t\bar{t}} \times B(t \to bW)^2$; if one trusts QCD and the NLO + NNLL rates, this measurement yields $B(t \to bW)$ to $\pm 5\%$ at Tevatron Run 2 and $\pm 3\%$ at the LHC. Second, measure the standard-model rate of single-top production, which is really $\sigma_{tX} \times B(t \to bW)$. The production

16 Jul 2003 16:50 AR AR199-NS53-09.tex AR199-NS53-09.sgm LaTeX2e(2002/01/18) P1: IKH

cross section, which is proportional to the partial width $\Gamma(t \to bW)$, is obtained by dividing out the known branching fraction. This is really a measurement of $g_W \times |V_{tb}|$. Assuming exact dependence on the standard-model gauge coupling g_W, this directly determines $|V_{tb}|$—to $\pm 12\%$ at the Tevatron (2 fb^{-1}) and $\pm 5\%$ at the LHC, where the measurement will be systematics-limited. The top-quark total width is then the partial width, given by Equation 17, divided by B. The precision will be similar to that for the partial width to bW.

For the total width measurement, it is expected that the three-generation value of $|V_{tb}|$ would be used, since it is known much more precisely from low-energy data than can be measured directly. The technique to measure $|V_{tb}|$ directly at hadron colliders simply establishes to a high degree of confidence that no fourth generation exists, which is already highly disfavored by electroweak precision data. One may also cross-check $B(t \to bW)$ by taking the ratio of dilepton to single-lepton events in $t\bar{t}$ production.

4.6. Yukawa Coupling

Yukawa couplings relate the matter content of the standard model to the source of mass generation, the Higgs sector. For the top quark in the standard model, this is written as a Lagrangian term $\mathcal{L} = -Y_t \bar{t}_L \phi t_R + \text{h.c.}$ When the Higgs field ϕ acquires a vacuum expectation value v, $\phi \to \frac{1}{\sqrt{2}}(v + H)$, the term proportional to v becomes the top-mass term and and the field term $-\frac{1}{\sqrt{2}} Y_t \bar{t}_L H t_R$ becomes the interaction of a pair of top quarks with the physical Higgs boson. Thus, the top-quark mass is fundamentally related to the Higgs vacuum expectation value and its Yukawa coupling, $m_t = Y_t\, v/\sqrt{2}$. Because $v/\sqrt{2} = 246$ GeV and $m_t = 174.3$ GeV, it appears that Y_t is exactly 1, a provocative value, leading to speculation that important new physics may be accessed via top-quark studies. The task then is to verify that $Y_t = 1$ by probing the Higgs-top interaction and thereby the mechanism of fermion mass generation. The top-Higgs coupling turns out to be the most difficult top-quark property to measure!

v = 246 GeV

There are three methods to consider at hadron colliders: (*a*) inclusive Higgs production, $gg \to H$, mediated dominantly by a top-quark loop; (*b*) associated production with a single top quark; or (*c*) associated production with a pair. Of these, $gg \to H$ has the largest cross section, but it is only minimally useful. First, there is the possibility that additional undiscovered particles mediate a loop contribution, which may not be separable. Second, in 2HDM scenarios, the bottom-quark contribution introduces an additional uncertainty because it must be separated. Although this channel is still useful, direct access to Y_t via top-quark associated production is more attractive.

One would expect the cross section for tH production to be larger than that for $t\bar{t}H$, which is more than two orders of magnitude smaller than $gg \to H$ owing to phase-space suppression, since there is more phase space available with only one top quark. Unfortunately, a unitarity cancellation between tH diagrams (131) renders this channel useless. It was hoped that the unique signature of $t\bar{t}(H \to b\bar{b})$

would make it observable—for a light Higgs boson—at the Tevatron (132). However, unexpectedly large, negative QCD NLO corrections (133) have all but quashed this hope. At the LHC, $t\bar{t}(H \rightarrow b\bar{b})$ is probably visible for a very light Higgs (134), and it would be possible to observe $t\bar{t}(H \rightarrow W^+W^-)$ for Higgs masses larger than ~ 120 GeV (126, 135). The statistical uncertainty on Y_t for the latter could be as small as 10%, but the systematic uncertainties have not been estimated.

At hadron colliders, simply measuring any of these production rates is not sufficient to measure Y_t, despite the commonly held belief that $t\bar{t}H$ grants "direct access" to the top-quark Yukawa coupling. The cross section is a convolution of Y_t and the Higgs-boson branching ~~ratio~~, which is a priori unknown. Only by multiple Higgs measurements that determine all the Higgs branching ~~ratios~~ can such a cross-section measurement determine Y_t. Thus, this aspect of top-quark physics is inextricably linked to Higgs physics. At the LHC, where a Higgs signal would not be so statistically limited and would appear in multiple channels, branching ratios can be determined indirectly with mild theoretical assumptions (136), making interpretation of the rates useful. However, an unbiased measurement of Y_t will almost certainly require additional Higgs data from a linear collider. There is an important exception to this requirement for the case of a large excess of events: ~~Even~~ if the branching ~~ratio~~ to the observed final state is assumed to be unity, strong constraints can be put on models where Y_t is significantly enhanced over standard-model expectations. This can happen, e.g., in topcolor-assisted technicolor (TC2) models (137).

5. SUMMARY

Discovery of the top quark has opened up a rich field of physics that is justifiably attracting much attention. Careful examination of the top quark's production and decay characteristics, and precision measurement of its mass and other properties, are needed to test the standard model. Theoretical and experimental efforts must proceed hand-in-hand to this end. The top quark may lead to the discovery of new physics: its large mass may well indicate a special role in electroweak- and flavor-symmetry breakings, and particles yet unobserved may show up in its production or decay. It is also important to understand top-quark events as fully as possible because they will constitute a strong background to many potential new-physics signals in other searches.

Following are the 10 most important studies of the top quark to be performed at hadron colliders in the foreseeable future:

1. mass
2. pair-production cross section (via strong interaction)
3. single-production cross section (via weak interaction)

insert comma after each item

insert comma after each item

4. the CKM matrix elements involving the top quark and the standard-model branching fractions $B(t \to bX)$ and $B(t \to qW)$
5. total width[13]
6. spin (or spin correlation between pair-produced top quarks)
7. decay angular distributions and W helicity in top decays
8. kinematic distributions of top quarks in single and pair production
9. search for new resonaces in the $t\bar{t}$ invariant mass spectrum
10. search for new physics in production and decay modes that are either highly suppressed or nonexistent in the standard model but could be signficantly enhanced in alternative or extended models (obviously, this overlaps with all of the preceding)

insert period after the last item

For the next five years or so, direct study of the top quark belongs to the ongoing Run 2 of the Tevatron. Collider upgrades have resulted in a higher rate of production through increases in energy (resulting in a cross-section enhancement of about 40% for pairs and 60% for single top quarks compared with Run 1) and integrated luminosity (50 times or more). Detector upgrades will allow superior background suppression. We expect that data samples containing perhaps 100 times as many top quarks as presently available will be collected during this period. After that, the LHC will dominate the field, delivering another hundredfold increase in top-quark yield. Better understanding of QCD dynamics is required to make full use of the rich statistics of top-quark events at hadron colliders, leaving plenty of room for work to prepare for the LHC era. High-energy physicists around the world have started planning for a future e^+e^- linear collider, which may become operational around 2015. Such a machine will offer new means for precision studies of the top-quark properties and dynamics.

In closing, we quote an observant colleague (138): "In physics, one discovery often leads to others. Top opens a new world—the domain of a very heavy fermion—in which the strange and wonderful may greet us."

ACKNOWLEDGMENTS

We thank the following people for invaluable advice: Jerry Blazey, Arnd Brandenburg, Tom Ferbel, Mark Kruse, Eric Laenen, Michelangelo Mangano, Steve Martin, Carlo Oleari, Lynne Orr, Stephen Parke, John Parsons, Rob Roser, Zack Sullivan, and Scott Willenbrock. DC's work was supported in part by a grant from the U.S. National Science Foundation, and JK's by the U.S. Department of Energy. DR would like to thank Fermilab and DESY, where parts of this work were completed.

[13]A model-independent precise and direct measurement of the top-quark total width will have to await threshold scans of electroweak Drell-Yan production of top-antitop pairs at a future e^+e^- linear collider.

The *Annual Review of Nuclear and Particle Science* is online at http://nucl.annualreviews.org

LITERATURE CITED

1. Abe F, et al. (CDF Collab.) *Phys. Rev. D* 50:2966 (1994); *Phys. Rev. Lett.* 74:2626 (1995); Abachi S, et al. (DØ Collab.) *Phys. Rev. Lett.* 74:2632 (1995)
2. Abazov VM, et al. (DØ Collab.) *Phys. Rev. D* 67:012004 (2003); Affolder T, et al. (CDF Collab.) *Phys. Rev. D* 64:032002 (2001); Abe F, et al. (CDF Collab.) *Phys. Rev. Lett.* 80:2773 (1998); Abachi S, et al. (DØ Collab.) *Phys. Rev. D* 58:05200 (1998); Abe F, et al. (CDF Collab.) *Phys. Rev. Lett.* 79:3585 (1997); Abachi S, et al. (DØ Collab.) *Phys. Rev. Lett.* 79:1203 (1997)
3. Abe F, et al. (CDF Collab.) *Phys. Rev. D* 59:092001 (1999)
4. Abachi S, et al. (DØ Collab.) *Phys. Rev. Lett.* 79:1197 (1997); Abbott B, et al. (DØ Collab.) *Phys. Rev. D* 58:052001 (1998);
5. Estrada J, (DØ Collab.) hep-ex/0302031
6. Abbott B, et al. (DØ Collab.) *Phys. Rev. Lett.* 80:2063 (1998); Phys. Rev. D 60:052001 (1999)
7. Demortier L, et al. (CDF and DØ Collabs.) Fermilab-TM-2084 (1999)
8. Abe F, et al. (CDF Collab.) *Phys. Rev. Lett.* 80:2676 (1998); *Phys. Rev. Lett.* 80:2767 (1998); *Phys. Rev. Lett.* 80:2779 (1998); *Phys. Rev. Lett.* 82:271 (1999); erratum, *Phys. Rev. Lett.* 82:2808 (1999)
9. Affolder T, et al. (CDF Collab.) *Phys. Rev. Lett.* 84:216 (2000)
10. Abbott B, et al. (DØ Collab.) *Phys. Rev. Lett.* 85:256 (2000)
11. Affolder T, et al. (CDF Collab.) *Phys. Rev. D* 65:91102 (2002)
12. Abbott B, et al. (DØ Collab.) *Phys. Lett. B* 517:282 (2001) 11
13. Abbott B, et al. (DØ Collab.) *Phys. Rev. Lett.* 82:4975 (1999); Abazov VM, et al. (DØ Collab.) *Phys. Rev. Lett.* 88:151803 (2002)
14. Abe F, et al. (CDF Collab.) *Phys. Rev. Lett.* 79:4975 (1997); Affolder T, et al. (CDF Collab.) *Phys. Rev. D* 62:012004 (2000)
15. Abe F, et al. (CDF Collab.) *Phys. Rev. Lett.* 80:2525 (1998) 14
16. Hagiwara K, et al. (Particle Data Group). *Phys. Rev. D* 66:010001 (2002)
17. Kane GL. *Mexico City HE Phenom.* 1991:0241–89 (1991)
18. Murayama H, Peskin ME. *Annu. Rev. Nucl. Part. Sci.* 46:533 (1996)
19. Accomando E, et al. (ECFA/DESY LC Physics Working Group Collab.) *Phys. Rep.* 299:1 (1998)
20. Beneke M, et al. hep-ph/0003033
21. Abe F, et al. (CDF Collab.) *Nucl. Instrum. Methods Phys. Res., Sect. A* 271:387 (1988); Abe F, et al. (CDF Collab.) *Nucl. Instrum. Methods Phys. Res., Sect. A* 350:73 (1994); Abachi S, et al. (DØ Collab.) *Nucl. Instrum. Methods Phys. Res., Sect. A* 338:185 (1994) 19
22. Newman-Holmes C (CDF Collab.) Fermilab-Conf-96/218-E (1996); Blair R, et al. (CDF Collab.) Fermilab-Conf-96/390-E (1996); Abachi S, et al. (DØ Collab.) Fermilab-Pub-96/357-E (1996)
23. ATLAS Collab. *ATLAS Detector and Physics Performance Technical Design Rep.,* CERN/LHCC 99-14/15 (1999); *CMS letter of intent,* CERN/LHCC 92-3(1992)90; Iashvili I, et al. CMS TN/92-34Y (1992)
24. Bhat PC, Prosper HB, Snyder SS. *Int. J. Mod. Phys.* A13:5113 (1998)
25. Wimpenny SJ, Winer BL. *Annu. Rev. Nucl. Part. Sci.* 46:149 (1996)
26. Campagnari C, Franklin M. *Rev. Mod. Phys.* 69:137 (1997)
27. Bernreuther W, et al. *Int. J. Mod. Phys.* A18:1357 (2003)

28. Bonciani R, et al. *Nucl. Phys. B* 529:424 (1998), updated in Cacciavi M, et al. hep-ph/0303085
29. Kidonakis MN, et al. *Phys. Rev. D* 64:114001 (2001)
30. Catani S, et al. *Phys. Lett.* B378:329 (1996)
31. Beenakker W, et al. *Nucl. Phys. B* 411:343 (1994)
32. Sjöstrand T, *Comp. Phys. Comm.* 82:74 (1994) 26
33. Marchesini G, et al. *Comp. Phys. Comm.* 67:465 (1992); Corcella G, et al. *JHEP* 0101:10 (2001)
34. Paige FE, Protopopescu SD. BNL-29777 (1981); Baer H, et al. ISAJET 7.48, hep-ph/0001086
35. Mrenna S, Yuan C-P. *Phys. Rev. D* 55:120 (1997)
36. Orr LH, Stelzer T, Stirling WJ. *Phys. Rev. D* 56:446 (1997) 30
37. Frixione S, et al. *Phys. Lett.* B351:555 (1995)
38. Barger VD, Phillips RJ. *Collider Physics.* Redwood City, CA: Addison-Wesley (1987) 58
39. Barnett RM, Hall LJ. *Minneapolis 1996, Particles and Fields* 1:192
40. Sullivan Z. *Snowmass 1996, New Directions for High-Energy Physics,* p. 797. http://www.slac.stanford.edu/pubs/snowmass96/PDF/STC126.PDF
41. Smith MC, Willenbrock S. *Phys. Rev. D* 54:6696 (1996)
42. Mrenna S, Yuan C-P. *Phys. Lett.* B416:200 (1998)
43. Harris BW, et al. *Phys. Rev. D* 66:054024 (2002)
44. Maltoni F, Sullivan Z, Willenbrock S. ~~hep-ph/0301033;~~ Plehn T. *Phys. Rev. D* 67:014018 (2003) and references therein
45. Stelzer T, Sullivan Z, Willenbrock S. *Phys. Rev. D* 58:094021 (1998)
46. Bordes G, van Eijk B. *Nucl. Phys. B* 435:23 (1995) 37
47. Stelzer T, Sullivan Z, Willenbrock S. *Phys. Rev. D* 56:5919 (1997) 38
48. Tait T, Yuan C-P. *Phys. Rev. D* 63:014018 (2001)
49. Heinson AP, Belyaev AS, Boos EE. *Phys. Rev. D* 56:3114 (1997); Tait T. *Phys. Rev. D* 61:034001 (2000); Belyaev AS, Boos EE. *Phys. Rev. D* 63:034012 (2001) Belyaev AS, Boos EE, Dudko LV. *Phys. Rev. D* 59:075001 (1999)
50. Lane K. *Phys. Rev. D* 52:1546 (1995)
51. Eichten E, Lane K. *Phys. Lett.* B327:129 (1994) 42
52. Hill CT, Parke SJ. *Phys. Rev. D* 49:4454 (1994) 43
53. Harris RM, Hill CT, Parke SJ. hep-ph/9911288
54. Casalbuoni R, et al. *Z. Phys. C* 69:519 (1996)
55. Holdom B, Ramana MV. *Phys. Lett.* B353:295 (1995)
56. Popovic MB, Simmons EH. *Phys. Rev. D* 62:035002 (2000)
57. Appelquist T, Cheng H, Dobrescu B. *Phys. Rev. D* 64:035002 (2001) Appelquist T, Triantaphyllou G. *Phys. Rev. Lett.* 69:2750 (1992)
58. Cho PL, Simmons EH. *Phys. Rev. D* 51:2360 (1995)
59. Atwood D, Kagan A, Rizzo TG. *Phys. Rev. D* 52:6264 (1995)
60. Eichten E, Lane KD, Peskin ME. *Phys. Rev. Lett.* 50:811 (1983)
61. Lane KD, Eichten E. *Phys. Lett.* B352:382 (1995)
62. Hill CT. *Phys. Lett.* B266:419 (1991)
63. Hill CT. *Phys. Lett.* B345:483 (1995); Balaji B. *Phys. Lett.* B393:89 (1997)
64. Simmons EH. *Phys. Rev. D* 55:494 (1997)
65. Affolder T, et al. (CDF Collab.) *Phys. Rev. Lett.* 85:2062 (2000);
66. Affolder T, et al. (CDF Collab.) *Phys. Rev. Lett.* 87:102001 (2001)
67. ~~Jain S (for the DØ Collab.) hep-ex/0302037~~
68. Abe F, et al. (CDF Collab.) *Phys. Rev. D* 59:092001 (1999)
69. Carlson DO, Yuan C-P. *Phys. Lett.* B306:386 (1993)

70. Carlson DO, Malkawi E, Yuan C-P. *Phys. Lett.* B337:145 (1994)
71. Hikasa KI, et al. *Phys. Rev. D* 58:114003 (1998)
72. Boos EE, Dudko LV, Ohl T. *Eur. Phys. J. C* 11:473 (1999)
73. Atwood D, et al. *Phys. Rev. D* 54:5412 (1996)
74. Li CS, et al. *Phys. Rev. D* 57:2009 (1998)
75. Li CS, et al. *Phys. Lett.* B398:298 (1997)
76. Bar-Shalom S, Atwood D, Soni A. *Phys. Rev. D* 57:1495 (1998)
77. Malkawi E, Tait T, Yuan C-P. *Phys. Lett.* B385:304 (1996); He HJ, Tait T, Yuan C-P. *Phys. Rev. D* 62:011702 (2000)
78. Oakes RJ, et al. *Phys. Rev. D* 57:534 (1998)
79. Han T, et al. *Phys. Rev. D* 58:073008 (1998)
80. Malkawi E, Tait T. *Phys. Rev. D* 54:5758 (1996)
81. Tait T, Yuan C-P. *Phys. Rev. D* 55:7300 (~~1994~~ 1996)
82. Glashow SL, Iliopoulos J, Maiani L. *Phys. Rev. D* 2:1285 (1970) 72
83. Peccei R, Zhang X. *Nucl. Phys. B* 337:269 (1990); Kane G, Yuan C-P, Ladinsky D. *Phys. Rev. D* 45:124 (1992); Jezabek M, Kuhn JH. *Phys. Lett.* B329:317 (1994); Nelson CA, et al. *Phys. Rev. D* 56:5928 (1997) 73
84. Dalitz RH, Goldstein GR. *Proc. R. Soc. London A* 445:2803 (1999)
85. Affolder T, et al. (CDF Collab.) *Phys. Rev. Lett.* 86:3233 (2001)
86. Kilminster B. *Testing V-A in top decays at CDF.* Presented at Conf. Intersections of Particle and Nuclear Physics, 2003 (CIPANP 2003), New York City, May 19–24
87. Mahlon G, Parke S. *Phys.Lett.* B347:394 (1995)
88. Yue C, et al. *Phys. Rev. D* 64:095004 (2001); Diaz-Cruz JL, et al. *Phys. Rev. D* 41:891 (1990); Eilam G, Hewett J, Soni A. *Phys. Rev. D* 44:1473 (1991) 77
89. Frey R, et al. *Snowmass 1996, New Directions for High-Energy Physics,* p. 760 (1997); Aguilar-Saavedra JA, Branco GC. *Phys. Lett.* B495:347 (2000) 78
90. Gunion JF, et al. *The Higgs Hunter's Guide.* Redwood City, CA: Addison-Wesley (1990)
91. ALEPH, DELPHI, L3, and OPAL Collabs. hep-ex/0107030
92. ALEPH, DELPHI, L3, and OPAL Collabs. hep-ex/0107031
93. Alam MS, et al. (CLEO Collab.) *Phys. Rev. Lett.* 74:2885 (1995)
94. Carena M, et al. hep-ph/0010338
95. Luke M, Savage, MJ. *Phys. Lett.* B307:387 (1993) 83
96. Diaz-Cruz JL, et al. *Phys. Rev. D* 60:115014 (1999)
97. Hosch M, et al. *Phys. Rev. D* 58:034002 (1998); Mahlon G, Kane GL. *Phys. Rev. D* 55:2779 (1997); Ambrosiano S, et al. *Phys. Rev. D* 54:5395 (1996); Mrenna S, Yan CP. *Phys. Lett.* B367:188 (1996); Sender J. *Phys. Rev. D* 54:3271 (1996); Wells JD, Kane GL. *Phys. Rev. Lett.* 76:869 (1996)
98. Affolder T, et al. (CDF Collab.) *Phys. Rev. D* 63:091101 (2001)
99. Agashe K, Graesser M. *Phys. Rev. D* 54:4445 (1996); Yang JM, Young B-L, Zhang X. *Phys. Rev. D* 58:055001 (1998); Han T, Magro MB. *Phys. Lett.* B476:79 (2000); Eilam G, et al. *Phys. Lett.* B510:227 (2001); Abraham KJ, et al. *Phys. Rev. D* 63:034011 (2001)
100. Weinberg S. *Phys. Rev. D* 19:1277 (1979); Susskind L. *Phys. Rev. D* 20:2619 (1979) 9
101. Dimopoulos S, Susskind L. *Nucl. Phys. B* 155:237 (1979); Eichten E, Lane K. *Phys. Lett.* B90:125 (1980) 10
102. Applequist T, et al. *Phys. Lett.* B220:223 (1989); Takeuchi T. *Phys. Rev. D* 40:2697 (1989); Miransky VA, Yamawaki K. *Mod. Phys. Lett.* A4:129 (1989); Matumoto K. *Prog. Theor. Phys.* 81:277 (1989); Chivukula RS, Cohen AG, Lane K. *Nucl. Phys. B* 343:554 (1990)

103. Aguilar-Saavedra JA, et al. (ECFA/DESY LC Phys. Work. Group Collab.) hep-ph/0106315; Abe T, et al. (Am. Linear Collider Phys. Group) *Linear Collider Physics Resource Book*, http://www.slac.stanford.edu/grp/th/LCBook/; Abe K, et al. *Physics at JLC,* http://lcdev.kek.jp/
104. Tollefson K, Varnes EW. *Annu. Rev. Nucl. Part. Sci.* 49:435 (1999)
105. Affolder T, et al. (CDF Collab.) *Phys. Rev. D* 63:032003 (2001)
106. Orr LH, Stelzer T, Stirling WJ. *Phys. Rev. D* 56:446 (1997); Orr LH, Stelzer T, Stirling WJ. *Phys. Rev. D* 52:124 (1995); Orr LH, Stelzer T, Stirling WJ. *Phys. Lett.* B354:442 (1995); Orr LH, Andre T, Stelzer T. *Vancouver 1998, High-Energy Phys*. 2:1103
107. Abe F, et al. (CDF Collab.) *Phys. Rev. Lett.* 79:1992 (1997)
108. Kondo K. *J. Phys. Soc. Jpn.* 57:4126 (1988); *J. Phys. Soc. Jpn.* 60:836 (1991)
109. Abe F, et al. (CDF Collab.) *Phys. Rev. Lett.* 80:2779 (1998)
110. Kharchilava A. *Phys. Lett.* B476:73 (2000)
111. Corcella G, Mangano ML, Seymour MH. *JHEP* 0007:004 (2000)
112. Brandenburg A, Si ZG, Uwer P. *Phys. Lett.* B539:235 (2002)
113. Stelzer T, Willenbrock S. *Phys. Lett.* B374:169 (1996)
114. Mahlon G, Parke S. *Phys. Rev. D* 53:4886 (1996) *Phys. Lett.* B411:173 (1997)
115. Bernreuther W, et al. *Phys. Rev. Lett.* 87:242002 (2001); Bernreuther W, Brandenburg A, Si ZG. *Phys. Lett.* B483:99 (2000)
116. Kane GL, Ladinsky GA, Yuan C-P. *Phys. Rev. D* 45:124 (1992)
117. Nelson CA. *Eur. Phys. J. C* 19:323 (2001)
118. Parke S, Shadmi Y. *Phys. Lett.* 387:199 (1996)
119. Mahlon G, Parke S. *Phys. Rev. D* 55:7249 (1997); *Phys. Lett.* B476:323 (2000)
120. Boos EE, Sherstnev AV. *Phys. Lett.* B534:97 (2002)
121. Chang D, Chang WF, Ma E. *Phys. Rev. D* 59:091503 (1999)
122. Baur U, Buice M, Orr LH. *Phys. Rev. D* 64:094019 (2001)
123. Abe T, et al. (Am. Linear Collider Work. Group Collab.) *Proc. APS/DPF/DPB Summer Study on the Future of Particle Physics (Snowmass 2001)*, ed. N Graf, hep-ex/0106057
124. Atwood D, Aeppli A, Soni A. *Phys. Rev. Lett.* 69:2754 (1992); Atwood D, Kagan A, Rizzo TG. *Phys. Rev. D* 52:6264 (1995); Haberl P, Nachtmann O, Wilch A. *Phys. Rev. D* 53:4875 (1996)
125. Martinez R, Rodriguez JA. *Phys. Rev. D* 65:057301 (2002)
126. Maltoni F, Rainwater D, Willenbrock S. *Phys. Rev. D* 66:034022 (2002)
127. Larios F, Perez MA, Yuan C-P. *Phys. Lett.* B457:334 (1999)
128. Eilam G, et al. *Phys. Rev. Lett.* 66:3105 (1991); Mehen T. *Phys. Lett.* B417:353 (1998)
129. Affolder T, et al. (CDF Collab.) *Phys. Rev. Lett.* 86:3233 (2001)
130. Willenbrock S. *Santa Barbara 1997, Heavy-Flavor Phys.* p. 402
131. Maltoni F, et al. *Phys. Rev. D* 64:094023 (2001)
132. Goldstein J, et al. *Phys. Rev. Lett.* 86:1694 (2001),
133. Beenakker W, et al. *Phys. Rev. Lett.* 87:201805 (2001) Reina L, Dawson S. *Phys. Rev. Lett.* 87:201804 (2001); Reina L, Dawson S, Wackeroth D. *Phys. Rev. D* 65:053017 (2002); Dawson S, Orr LH, Reina L, Wackeroth D. *Phys. Rev. D* 67:071503 (2003)
134. Richter-Was E, Sapinski M. *Acta Phys. Polon. B* 30:1001 (1999); Drollinger V, Muller T, Denegri D. CMS-NOTE-2002-006, hep-ph/0201249
135. Kostioukhine V, et al. ATL-PHYS-2002-019
136. Zeppenfeld D, et al. *Phys. Rev. D* 62:013009 (2000)
137. Leibovich AK, Rainwater D. *Phys. Rev. D* 65:055012 (2002)
138. Quigg C. *Phys. Today* 5:20; expanded version at hep-ph/9704332

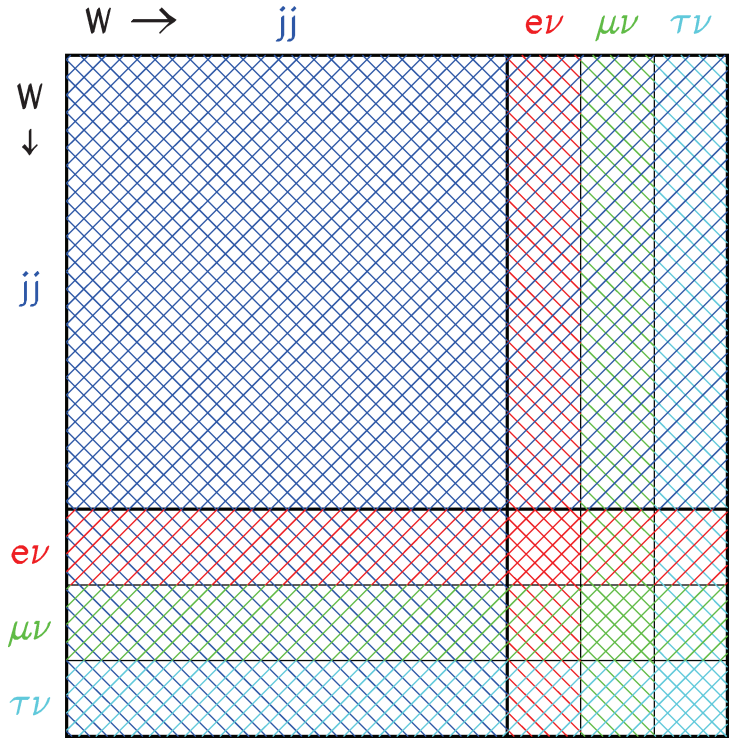

Figure 2 Branching fractions of $t\bar{t}$ due to the various subsequent W decays. All final states have an additional $b\bar{b}$ pair from the top decays.